



A record of impacts preserved in the lunar regolith

David L. Shuster^{a,*}, Greg Balco^{a,b,1}, William S. Cassata^{a,b,1}, Vera A. Fernandes^{a,b,1}, Ian Garrick-Bethell^{c,1,2}, Benjamin P. Weiss^{c,1}

^a Berkeley Geochronology Center, 2455 Ridge Road, Berkeley, CA 94709, USA

^b Department of Earth and Planetary Sciences, University of California - Berkeley, 307 McCone Hall, Berkeley, CA 94720-4767, USA

^c Department of Earth, Atmospheric and Planetary Sciences, Massachusetts Institute of Technology, 77 Massachusetts Avenue, Cambridge, MA 02139, USA

ARTICLE INFO

Article history:

Received 15 October 2009

Received in revised form 2 December 2009

Accepted 4 December 2009

Available online 13 January 2010

Editor: T.M. Harrison

Keywords:

Moon

lunar impacts

⁴⁰Ar/³⁹Ar thermochronometry

Apollo

regolith

ABSTRACT

The absolute chronology of meteoroid impacts on the Moon is largely quantified by only a few ⁴⁰Ar/³⁹Ar “plateau ages” of rocks thought to be associated with specific impact events (Stöffler et al., 2006). We demonstrate a more broadly applicable approach by using high-resolution ⁴⁰Ar/³⁹Ar thermochronometry to investigate the physical conditions responsible for partially reset K-Ar systems in lunar rocks. Seven rocks from Apollo 16 regolith sample 63503 have plateau ages of either 3.9 billion yr (Ga) or 4.2 Ga and all experienced varying degrees of partial resetting. Concordance between diffusion kinetics and the degree of resetting among all samples shows that these observations are best explained by a heating event 3.3 Ga ago that lasted between ~10³ s (at ~600 °C) and ~20 yr (at ~300 °C). We conclude that partial resetting of the K-Ar systems in these samples record an impact event ~3.3 Ga ago that mixed several preexisting ejecta units in the Cayley Plains. If partially reset ⁴⁰Ar/³⁹Ar ages of other lunar highland samples also constrain the timing of late-stage reheating associated with impact events, they constitute an additional record of impacts preserved in the lunar regolith. A review of existing datasets from this perspective reveals that episodic pulses in the impactor flux in the inner system are common, and most likely related to dynamical events in the asteroid belt or outer Solar System.

© 2009 Elsevier B.V. All rights reserved.

1. Introduction

The record of the inner Solar System impactor flux is poorly known. The impactor flux is generally believed to have been smoothly declining since at least ~4 Ga and approximately constant since ~2.8 Ga (Neukum et al., 2001; Stöffler and Ryder, 2001; Stöffler et al., 2006), but evidence has emerged that brief pulses of impactors have been delivered to the inner solar system from the asteroid belt (Dermott et al., 1991; Bottke et al., 2007; Nesvorný et al., 2007; Levison et al., 2009) which would affect both the cratering record and the conditions for the development of life on Earth. To obtain information about the chronology of the impactor flux, the Moon preserves a better record than Earth due to its relative geological quiescence over the last several billion years (Stöffler et al., 2006). Although the relative stratigraphy of lunar impact craters is decipherable from remote surface imagery (Wilhelms, 1987), quantifying the absolute chronology has remained a challenge even after the Apollo and Luna missions. The absolute ages of some relatively young impacts [<500 million yr (Ma) old] have been determined by surface exposure dating using cosmogenic radionuclides (Arvidson et al., 1975;

Turner, 1971). Absolute dating of older impact structures, particularly large impact basins, has relied primarily on Rb/Sr and ⁴⁰Ar/³⁹Ar plateau ages of impact breccias from the Apollo 14–17 sites and their assumed association with the Imbrium (Dalrymple and Ryder, 1993; Stadermann et al., 1991), Serenitatis (Dalrymple and Ryder, 1996) and Nectaris (Maurer et al., 1978; Stöffler et al., 1985; Norman et al., 2006) basins. The absolute ages of these basins have been combined with relative ages (Wilhelms, 1987) to quantify early epochs in lunar geologic history.

Because impact events generate heat and Ar diffusivity is relatively high in geologic materials, ⁴⁰Ar/³⁹Ar plateau ages have been used to date lunar impact events on the basis that the plateau age records complete loss of radiogenic ⁴⁰Ar (⁴⁰Ar*) during an impact [e.g., Maurer et al., 1978; Stöffler et al., 1985; Stadermann et al., 1991; Dalrymple and Ryder, 1993; Dalrymple and Ryder, 1996; Norman et al., 2006]. However, ⁴⁰Ar/³⁹Ar age spectra can also record open-system behavior and partial diffusive loss of ⁴⁰Ar* subsequent to initial closure (Turner et al., 1966) which could potentially result from impact heating (Bogard, 1995). Observed ⁴⁰Ar/³⁹Ar age spectra of lunar samples commonly show incomplete ⁴⁰Ar* retention manifested as partially reset (i.e., sub-plateau) ⁴⁰Ar/³⁹Ar ages in initial heating steps [e.g., Schaeffer and Husain, 1973; Jessberger et al., 1974; Maurer et al., 1978; Ryder et al., 1991; Dalrymple and Ryder, 1996; Norman et al., 2006]. In nearly all cases, authors attributed these observations to events like “⁴⁰Ar loss on the lunar surface” (Jessberger et al., 1974) or more specifically “post-crystallization reheating, probably by later impacts” [e.g., Norman et al.,

* Corresponding author. Tel.: +1 510 644 9200.
E-mail address: dshuster@bgc.org (D.L. Shuster).

¹ Authors are listed alphabetically.

² Now at the Department of Geological Sciences, Brown University, 324 Brook Street, Box 1846, Providence, RI 02912, USA.

2006]. They quantified plateau ages and either did not discuss the deviant data or did not ascribe any age significance to them. In one exception, partially reset $^{40}\text{Ar}/^{39}\text{Ar}$ ages were used to quantify the ~2.1 Ga age of the Autolycus impact structure (Ryder et al., 1991).

$^{40}\text{Ar}/^{39}\text{Ar}$ data have been used to constrain the thermal history of some extraterrestrial materials [e.g., Turner et al., 1966; Turner et al., 1971; Turner, 1979; McConville et al., 1988; Shuster and Weiss, 2005], but, as noted above, partially reset ages of lunar rocks have not been widely exploited for this purpose. One reason for this is the difficulty in establishing whether impact heating or some other process was responsible for partial resetting, which reflects the fact that past studies did not generally quantify Ar diffusion kinetics for the samples that were dated. Accurate kinetics is required to relate laboratory observations to geological thermal histories, and thus to quantitatively constrain the mean temperatures and durations over which late-stage $^{40}\text{Ar}^*$ loss may have occurred (Turner, 1971).

In this work, we precisely controlled and accurately measured the temperatures of Ar degassing steps to quantify Ar diffusion kinetics of each sample. This permits us to infer significantly more information than solely a plateau age by considering the spatial distribution of $^{40}\text{Ar}^*$ within a sample (Albarède 1978) and the physical conditions which resulted in the apparent distribution [e.g., Turner et al., 1971; Albarède 1978; Shuster and Weiss, 2005]. As discussed above, two aspects of stepped-heating $^{40}\text{Ar}/^{39}\text{Ar}$ thermochronometry make it well suited for dating lunar impact events: sensitivity to thermal disturbance, and ability to record open-system behavior and partial loss of daughter atoms. In this study, we combine $^{40}\text{Ar}/^{39}\text{Ar}$ analyses from multiple rocks taken from the Apollo regolith sample 63503, diffusion kinetics inferred from these analyses, and simple models for Ar diffusion to assess whether or not a single thermal disturbance can explain partial resetting of the K–Ar system in all samples. We show that the observations are best explained by a relatively short-duration heating event ~3.3 Ga ago. This event was most likely a meteoroid impact. Finally, we argue that if partially reset $^{40}\text{Ar}/^{39}\text{Ar}$ ages of other regolith samples also reflect impact heating, re-inspection of existing datasets may yield a much more extensive record of lunar impacts than available from plateau ages alone.

2. Sample 63503

Apollo 16 sample 63503 is the 2–4 mm diameter size fraction of bulk regolith sample 63500 (collected as one scoop) at Station 13, approximately 750 m southeast of the rim of the 50 Ma-old (Arvidson et al., 1975), 1.0 km diameter North Ray crater (Ulrich et al., 1981). North Ray crater formed in a ridge on the flank of Smoky Mountain near the border between the Cayley and Descartes formations. Although originally assigned to the Cayley Formation, the crater was interpreted after the mission to have formed in and excavated material from the Descartes unit (Stöffler et al., 1982; Spudis, 1984; Stöffler et al., 1985; Wilhelms, 1987). Although 63503 is generally associated with North Ray crater, because it was collected from the distal flank of the ejecta blanket it should theoretically sample the shallowest materials excavated (Stöffler et al., 1985) when the North Ray Crater formed possibly mixed with local surficial materials. 63500 has cosmogenic-nuclide exposure ages that range from the 50 Ma age of North Ray to 390 Ma (Schaeffer and Husain, 1973; Arvidson et al., 1975). Published petrology and $^{40}\text{Ar}/^{39}\text{Ar}$ geochronometry of rocks from 63500 (Schaeffer and Husain, 1973; Maurer et al., 1978; James, 1982) and other lines of evidence suggest that the Cayley plains are a mixture of Nectaris and Imbrium ejecta (Korotev, 1997) and include many lithological units (James, 1982).

We conducted high-resolution $^{40}\text{Ar}/^{39}\text{Ar}$ thermochronometry of seven different rocks from 63503. These include fragmented feldspathic breccias and anorthosites containing 80–95% plagioclase and variable amounts of apparently plagioclase composition impact melt. Our optical and electron microscopy (data not shown) indicate that each rock falls into one of the three general petrographic categories similar to those observed by Maurer et al. (1978) in another 63503 split. Samples

63503, 1, 3, and 4 are fragmented feldspathic breccias containing ~80% plagioclase by volume with clasts of partly metamorphosed gabbro, clasts with porphyritic or granulitic texture and clasts of what appear to be quenched impact melt. Samples 11 and 15 are unbrecciated but fractured anorthosites containing ~95% plagioclase. Samples 9a and 13 appear to be mostly impact-generated melt that was primarily composed of plagioclase prior to melting and contain fragments of unmelted plagioclase. Thus the dominant K and $^{40}\text{Ar}^*$ -containing phases in these samples are plagioclase and glass of plagioclase composition.

3. Methods

3.1. Analytical details

Using conventional methods of $^{40}\text{Ar}/^{39}\text{Ar}$ geochronometry, the seven samples were irradiated alongside the Hb3gr fluence monitor (Supplementary Table S1) for 100 h within a Cd shielded vessel in the OSU TRIGA reactor, primarily to induce ^{39}Ar from ^{39}K . Using feedback-controlled laser-heating with a 30 W diode laser (with a wavelength of 810 ± 10 nm), we then sequentially heated each sample contained in a small Pt–Ir packet (Cassata et al., 2009). We measured and controlled its temperature with an axially aligned single-color, optical pyrometer for a specified amount of time (typically 15 min). Using a set of independent calibrations, we corrected the pyrometer measurements for variation in the Pt–Ir packet emissivity as a function of temperature against a type-C thermocouple. Each step was controlled with precision and accuracy better than $\pm 5^\circ\text{C}$. We optimized the heating parameters to reach the set-point temperature within ~30 s without exceeding it, which is essential to accurately quantify diffusion kinetics. To aid in quantifying diffusion kinetics, the heating schedules also included multiple heating steps at the same temperature (see Section 5). After each heating step, the evolved gas was purified by a series of SAES® getters in an automated vacuum system and the isotopic spectrum of the residual Ar was automatically analyzed with an MAP-215 mass spectrometer. We corrected measured Ar for blank contributions, mass discrimination and nuclear reaction interferences as well as radioactive decay of ^{37}Ar and ^{39}Ar to calculate an $^{40}\text{Ar}^*/^{39}\text{Ar}$ age spectrum for each of the seven regolith fragments (Table S1). We used the Hb3gr hornblende neutron fluence monitor and age of 1073.6 ± 8.8 Ma to determine the *J*-value (Jourdan and Renne, 2007).

3.2. Quantifying Ar diffusion kinetics

We began by quantifying Ar diffusion kinetics from measured release fractions of ^{37}Ar and ^{39}Ar , the extraction temperatures and durations, and by assuming a single, spherical diffusion domain geometry and an initially uniform spatial distribution of these two isotopes (Fechtig and Kalbitzer, 1966). In a recent study of Ar diffusion kinetics in terrestrial plagioclase, Cassata et al. (2009) demonstrated that a transition in the diffusive properties of plagioclase observed at ~900–1000 °C is most likely related to structural or crystallographic changes resulting from laboratory heating. They also demonstrated that diffusion kinetics of Ar in plagioclase is better quantified by ^{37}Ar than by ^{39}Ar ; because Ca is a stoichiometric constituent of plagioclase and K is not, synthetic ^{37}Ar is more likely to be uniformly distributed than ^{39}Ar . For these reasons, we take diffusion kinetics calculated from ^{37}Ar released below 900 °C as the best representation of Ar diffusion kinetics (Table 1). For consistency, we show $^{40}\text{Ar}/^{39}\text{Ar}$ ratio evolution diagrams (i.e., age spectra) as a function of the cumulative ^{37}Ar release fraction ($\Sigma F^{37}\text{Ar}$). However, because diffusion kinetics inferred from both isotopes agree (see Supplementary Fig. S1), our subsequent interpretation of $^{40}\text{Ar}/^{39}\text{Ar}$ data is not strongly affected by our choice of ^{37}Ar as the volumic isotope. We incorporated the diffusion kinetics thus determined for each sample into numerical forward models for Ar ingrowth and diffusion that we describe below.

Table 1Summary of $^{40}\text{Ar}/^{39}\text{Ar}$ thermochronometry parameters for the single-domain models.

Sample	E_a (kJ/mol)	(+/-)	$\ln(D_0/a^2)$ ($\ln(\text{s}^{-1})$)	(+/-)	n	χ^2_v	Dt/a^2 ($\times 10^{-5}$)	(+)	(-)	Plateau (Ga)	(+/-)	Initial (Ga)	(+/-)
63503,1	144.4	2.6	6.50	0.36	20	4.99	354.8	182.2	125.7	3.87	0.03	3.35	0.08
63503,3	152.2	4.3	6.85	0.55	20	16.07	41.7	34.2	21.7	3.87	0.20	3.39	0.16
63503,4	157.4	5.6	7.45	0.74	15	9.62	25.7	11.4	8.7	4.19	0.07	3.60	0.10
63503,9a	155.2	2.8	5.22	0.40	16	4.24	1.6	4.2	1.5	4.21	0.18	3.92	0.18
63503,11	172.1	3.7	7.63	0.46	13	4.24	27.5	32.7	17.1	4.24	0.08	3.31	0.19
63503,13	145.4	2.2	5.28	0.30	20	4.86	125.9	103.2	65.6	4.30	0.18	3.39	0.10
63503,15	115.9	3.5	2.47	0.48	20	10.63	125.9	47.9	30.4	4.21	0.14	3.35	0.09

Errors in diffusion parameters [E_a and $\ln(D_0/a^2)$] are reported at the 1σ confidence level, as estimated from error-weighted linear regressions of ^{37}Ar data.

The number of points (n) and the fit statistic (reduced chi-squared, χ^2_v) correspond to the Arrhenius regressions.

The values of Dt/a^2 are quantified from the best-fitting agreement between a 3.3 Ga heating event model and the $^{40}\text{Ar}/^{39}\text{Ar}$ release data of each sample as determined from the minima in a fit statistic (also using χ^2_v) calculated for various Dt/a^2 values as shown in Figs. 1 and S1.

The asymmetric errors in Dt/a^2 (+ and -) are estimated from the values calculated at fixed distances (typically +1.2 in χ^2_v) above the best-fit solution.

All ages are calculated using the decay constant $\lambda_{40K} = 5.543 \times 10^{-10} \text{ yr}^{-1}$, and corrected for ^{37}Ar and ^{39}Ar decay using half lives of 35.2 days and 269 yr, respectively and nuclear reactor-produced interferences (Table S1). Age uncertainties include analytical error in J -value determined using fluence monitor Hb3gr (Table S1).

4. Results

Fig. 1 shows three examples of our $^{40}\text{Ar}/^{39}\text{Ar}$ thermochronometry results. Observed $^{40}\text{Ar}/^{39}\text{Ar}$ plateau ages and the Ar diffusion kinetics for all samples appear in Table 1; all seven datasets appear in Supplementary Table S1 and Supplementary Fig. S1. We observe plateau ages in each sample as well as: (i) different plateau ages in different rocks, (ii) sub-plateau ages in all initial steps, and (iii) concordant ages in the initial steps of different samples. For example, 63503,1 and 11 have different $^{40}\text{Ar}/^{39}\text{Ar}$ plateau ages (3.87 ± 0.03 Ga and 4.24 ± 0.08 Ga) but the initial steps of both analyses share a common age of ~ 3.3 Ga. Remarkably, out of these seven samples, five (63503,1,3,11,13 and 15) have initial step ages between 3.3 and 3.4 Ga despite different lithologies, textures, diffusion kinetics, and $^{40}\text{Ar}/^{39}\text{Ar}$ plateau ages (either ~ 3.9 Ga or ~ 4.2 Ga). The other two samples (63503,4 and 9a) have plateau ages ~ 4.2 Ga and initial step ages that are more similar to their plateau ages. These patterns indicate open-system behavior in the whole-rock K-Ar systems.

Diffusion coefficients [i.e., values of D/a^2] calculated from both ^{37}Ar and ^{39}Ar release fractions are in good agreement with one another in all cases (Supplementary Fig. S1). This simply reflects the observation that apparent K/Ca ratios are nearly constant through each release spectrum, and therefore that K and Ca are similarly sited in these samples. The apparent diffusion kinetics quantified by linear regression to steps below 900 °C are reported in Table 1 and are in good agreement with Ar diffusion kinetics of terrestrial plagioclase [Cassata et al. (2009) and references therein], further indicating that plagioclase is the dominant carrier of $^{40}\text{Ar}^*$ in these samples. Reasonably good agreement between values of $\ln(D/a^2)$ calculated from isothermal heating steps is consistent with the single-domain model used to calculate diffusion coefficients (see additional discussion below). More protracted retrograde heating cycles to lower temperatures would have better tested this model assumption, but the observed reproducibility in isothermal steps suggests that single values of E_a and the characteristic diffusive length scale (i.e., a) adequately characterize diffusive Ar mobility throughout K-bearing regions in each sample. We evaluate this more rigorously and consider the possibility of more complicated scenarios below (see Discussion).

Turner et al. (1972) showed that K-rich mesostasis with higher apparent K/Ca ratios in lunar mare basalts may have lower $^{40}\text{Ar}^*$ retentivity. Although we observe a weak correlation between step ages and $^{39}\text{Ar}/^{37}\text{Ar}$ ratios in some samples, our observations do not support this scenario for the 63503 feldspathic breccias and anorthositic. We observe (i) equal or greater variance (typically less than a factor of 2) in the Ca/K ratios of plateau-defining steps compared to the variance of the initial steps that deviate from the plateau (Supplementary Table S1), and (ii) insignificant differences between ^{37}Ar and ^{39}Ar Arrhenius relationships [e.g. Fig. 1(a–c)]. We

also find no correlation between the average Ca/K ratios and diffusion kinetics or Dt/a^2 value of each sample.

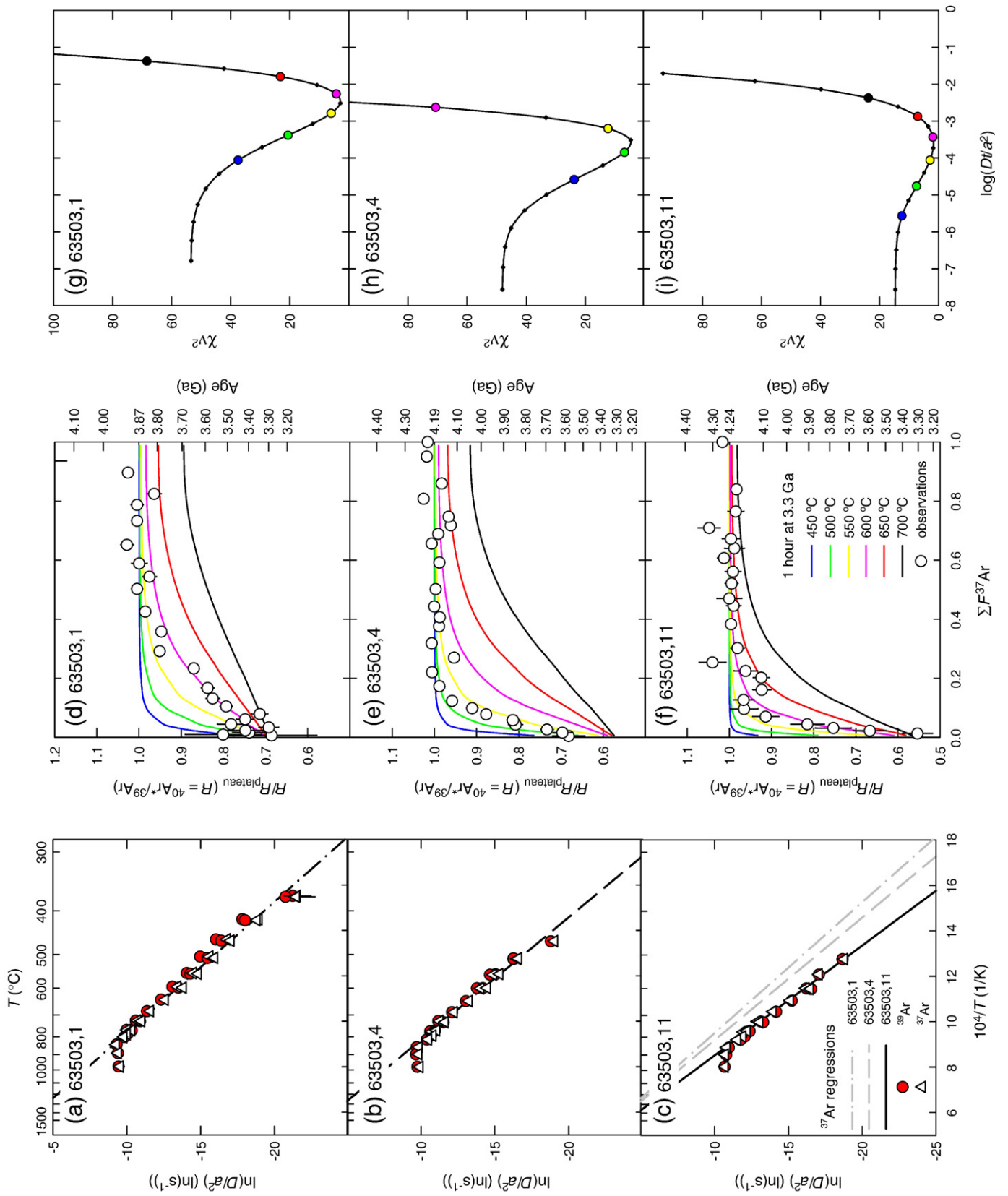
5. Discussion

5.1. A record of late-stage ^{40}Ar loss

Concordance in partially reset $^{40}\text{Ar}/^{39}\text{Ar}$ ages of these rocks constrains the timing of late-stage diffusive $^{40}\text{Ar}^*$ loss. The last time of significant $^{40}\text{Ar}^*$ loss must be equal to or younger than the initial step age. For example, if $^{40}\text{Ar}^*$ is currently being lost by diffusion, the initial $^{40}\text{Ar}/^{39}\text{Ar}$ ratio should indicate zero age regardless of chemical composition or any initial condition constrained by the plateau age. Concordance in initial step ages of different samples, however, strongly suggests that the concordant age directly quantifies the latest time of significant ^{40}Ar loss. By this reasoning, 3.3–3.4 Ga ages in initial heating steps of 63503 samples with different $^{40}\text{Ar}/^{39}\text{Ar}$ plateau ages (i.e., different crystallization or impact ages) suggest that the last significant loss of $^{40}\text{Ar}^*$ occurred 3.3–3.4 Ga ago.

A simple explanation for these results is that the seven distinct, yet spatially juxtaposed rocks experienced at least one common event ~ 3.3 Ga ago that partially reset the K-Ar system in each, and insignificant diffusive loss of $^{40}\text{Ar}^*$ occurred after this event. In addition, two observations strongly support this hypothesis. First, there exist small but significant differences in the temperature-dependent Ar diffusion kinetics, $D(T)/a^2$, quantified as described above by linear Arrhenius relationships. Second, initial steps of samples with higher diffusivity at lower temperatures are more deviated from corresponding $^{40}\text{Ar}/^{39}\text{Ar}$ plateau ages (Fig. 1). Less retentive samples (e.g., 63503,1 and 15) more tightly constrain the latest age of significant heating (an extreme case would result in a reset plateau age). Samples with highest retentivity (e.g., 63503,9 and 11) show the least deviation from the plateau age. These observations support the assumption that diffusion kinetics determined in the laboratory are an inherent property predicting the total $^{40}\text{Ar}^*$ lost from each sample and are consistent with the single thermal event hypothesis.

Although in detail we do not expect these different samples to have shared exactly the same thermal conditions 3.3 Ga ago, our objective in the following discussion is to test whether their data are adequately predicted by a thermal event with a duration and temperature common to all samples at that time. Furthermore, we seek to accomplish this with the simplest set of assumptions and the fewest free parameters needed to adequately explain the observations. We therefore assume that: (i) the $^{40}\text{Ar}/^{39}\text{Ar}$ release spectra reflect the spatial distribution of radiogenic ^{40}Ar in each sample; (ii) each distribution resulted solely from radiogenic ingrowth and diffusive loss of $^{40}\text{Ar}^*$ since the time defined by the $^{40}\text{Ar}/^{39}\text{Ar}$ plateau age, and (iii) the Ar diffusion kinetics and apparent diffusive length



scales determined from our experimental results apply throughout the history of the samples. By using whole-rock, linear Arrhenius regressions, we effectively assume the data reflect plagioclase crystals or fragments, which collectively contain well-defined diffusion kinetics. Finally, we take the time of the thermal event to be the youngest initial step age in the sample set (3.3 Ga) rather than the mean (3.47 Ga) of seven initial ages. This is simply because, as discussed above, given a uniform K distribution in a grain, the initial step age is strictly an upper bound on the age of the resetting event. As the samples with highest apparent Ar retentivity are less perturbed (Fig. 1), complete loss of $^{40}\text{Ar}^*$ from the edges of diffusion domains may not have occurred in all samples.

We constructed a numerical forward model for $^{40}\text{Ar}^*$ ingrowth and diffusion that incorporates these assumptions and has one free parameter, the non-dimensional diffusion time Dt/a^2 of the thermal event at 3.3 Ga. Fitting this model to each observed $^{40}\text{Ar}/^{39}\text{Ar}$ spectrum by minimizing the error-weighted sum of squared residuals between modeled and measured $^{40}\text{Ar}/^{39}\text{Ar}$ over all heating steps [represented by the reduced chi-squared statistic (χ^2_v) shown in Fig. 1], yielded a best-fitting value of Dt/a^2 for each sample (Fig. 1 and Supplementary Fig. S1). Because D is temperature-dependent, a particular value of Dt/a^2 corresponds to a solution set of duration and temperature (t - T) combinations which would all equivalently yield the observed disturbance of a given sample's $^{40}\text{Ar}^*$ spatial distribution; these are represented as curves in Fig. 2. Differences in diffusion kinetics and the degree of $^{40}\text{Ar}^*$ loss cause these curves to intersect, making it theoretically possible to find a unique solution for the duration and temperature of the thermal event [e.g., Reiners, 2009].

5.2. Identifying the best-fit solution

We obtained a best-fit solution for the duration and temperature of the 3.3 Ga thermal event as follows (Fig. 2). From each of the seven analyses ($k=1\dots n$; in this case $n=7$) we quantified the three parameters: activation energy $(E_a)_k$ and diffusivity at infinite temperature $(D_o/a^2)_k$ from the ^{37}Ar Arrhenius regressions (e.g., Fig. 1a–c), and the non-dimensional characteristic “diffusion time” $(Dt/a^2)_k$ found by matching forward diffusion models for a heating event 3.3 Ga ago to the observed $^{40}\text{Ar}/^{39}\text{Ar}$ spectra (e.g., Fig. 1d–f; Table 1). We sought the values and uncertainties for the two parameters T (temperature) and t (duration) of the 3.3 Ga event that best-fit all samples. T and t are related to observed values of $(E_a)_k$, $(D_o/a^2)_k$ and $(Dt/a^2)_k$ according to:

$$(Dt/a^2)_k = t \cdot (D_o/a^2)_k \cdot e^{-(E_a)_k/RT}. \quad (1)$$

Thus, the best-fitting values of T and t are those that minimize the χ^2_v statistic that compares the values of $(Dt/a^2)_k$ observed for each sample to those predicted by a particular t - T pair:

$$\frac{1}{n-2} \sum_{k=1}^n \frac{[(Dt/a^2)_k - t \cdot (D_o/a^2)_k \cdot e^{-(E_a)_k/RT}]^2}{\delta(Dt/a^2)_k^2}. \quad (2)$$

Fig. 1. Representative $^{40}\text{Ar}/^{39}\text{Ar}$ thermochronometry of individual rocks from Apollo 16 regolith sample 63503. (a–c) Diffusivity as a function of temperature (Arrhenius plot) calculated from ^{37}Ar and ^{39}Ar data for 63503,1 (a), 63503,4 (b), and 63503,11 (c). Points are diffusion coefficients calculated (Fechtig and Kalbitzer, 1966) using measured ^{39}Ar (circles) and ^{37}Ar (triangles) release fractions. The lines are the model $D(T)/a^2$ obtained from the linear regressions to ^{37}Ar data collected below 900 °C (above which an apparent material transition initiates in plagioclase (Cassata et al., 2009)) and used to calculate the curves shown in d–f, respectively, for each sub-sample. $D(T)$ is the diffusivity of Ar as a function of temperature T and a is the radius of the model diffusion domain. (d–f) Measured and modeled $^{40}\text{Ar}^*/^{39}\text{Ar}$ ratio evolution spectra for 63503,1 (d), 63503,4 (e), and 63503,11 (f). $^{40}\text{Ar}^*$ represents radiogenic ^{40}Ar , corrected for blank, mass discrimination and nuclear reactor-produced interferences to the measured ^{40}Ar signals. Circles are the measured $^{40}\text{Ar}^*/^{39}\text{Ar}$ ratios (R) normalized to the mean ratio of the plateau (R_{plateau}) with associated uncertainties plotted versus the cumulative ^{37}Ar release fraction ($\Sigma F^{37}\text{Ar}$). Also shown as curves are modeled release spectra using a spherical, one-domain model for heating at 3.3 Ga lasting 1 h from the present mean lunar surface temperature (-25°C) to various constant temperatures; these models correspond to specific values of Dt/a^2 . (g–i) The reduced chi-squared (χ^2_v) fit statistics for various model heating events at 3.3 Ga plotted versus values of $\log(Dt/a^2)$ for 63503,1 (g), 63503,4 (h), and 63503,11 (i). The best-fit value of Dt/a^2 for each sample is identified at the minimum χ^2_v value; colored points correspond to temperatures shown in panels (d–f), small black points indicate explicitly modeled conditions, and curves are polynomial fits to the χ^2_v values used to identify the minimum and uncertainty in Dt/a^2 . Equivalent figures for all seven samples appear in Fig. S1.

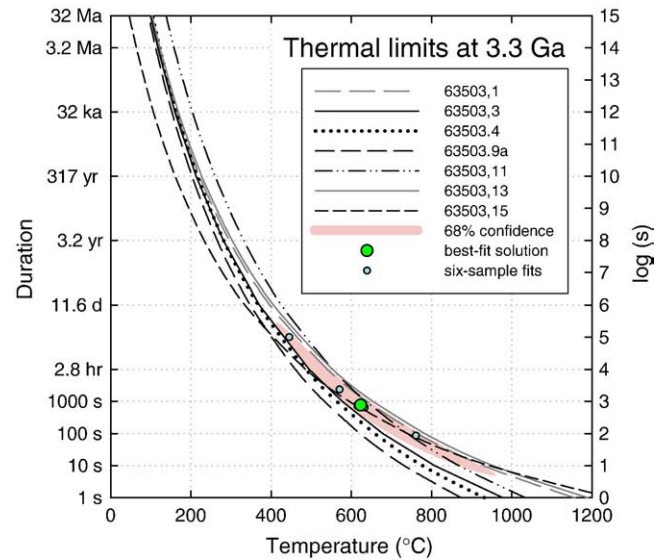


Fig. 2. Duration–temperature constraints on a thermal excursion experienced by 63503 at 3.3 Ga. The constraint is derived from the entire $^{40}\text{Ar}/^{39}\text{Ar}$ dataset of seven rocks from sample 63503. The solution set of duration and temperature (t - T) combinations shown as curves of constant Dt/a^2 were constrained by independently observed $^{40}\text{Ar}/^{39}\text{Ar}$ age spectra and Ar diffusion kinetics of the seven sub-samples (Figs. 1 and S1). Each curve indicates the t - T combinations at 3.3 Ga that result in the observed $^{40}\text{Ar}/^{39}\text{Ar}$ spectrum of each rock using a single-domain diffusion model. The green point is the best-fit solution to all seven ($t \sim 10^3$ s, $T \sim 600^\circ\text{C}$). The 68% confidence region on this solution is shown as a red ellipse (see Methods). The blue points are solutions calculated from each of the data subsets including only 6 samples; note that some are occluded by the best-fit solution symbol. These solutions demonstrate that the best-fit solution is not strongly influenced by any one particular dataset.

Because relative uncertainties in the inferred values of $(Dt/a^2)_k$ are significantly larger than those for $(E_a)_k$ and $(D_o/a^2)_k$, we have simplified the problem by using the uncertainty in the diffusion times [$\delta(Dt/a^2)_k$] alone to approximate the total uncertainty in all three observed parameters. As shown in Fig. 1, the best-fitting value of $(Dt/a^2)_k$ for each sample is that which minimizes χ^2_v relative to the measured $^{40}\text{Ar}/^{39}\text{Ar}$ spectrum. We estimated the uncertainty in $(Dt/a^2)_k$, [i.e., $\delta(Dt/a^2)_k$], from the range of values of $(Dt/a^2)_k$ for which χ^2_v is below a critical value obtained from statistical tables [e.g., (Bevington and Robinson, 1992); these values depend on the number of data but are generally near a value of 1]. These uncertainties are asymmetric about the best-fitting value, so we took account of this asymmetry in applying Eq. (2). We found the values of t and T that minimize Eq. (2) using the MATLAB® implementation of the Nelder–Mead simplex method (Lagarias et al., 1998). In a similar fashion as described above, we approximated the 68% confidence region about the best-fitting values by calculating a contour around the best-fit solution in the t - T grid located at a standard distance above the minimum value (Fig. 2; minimum $\chi^2_v=3.5$; χ^2_v of 68% confidence bound = 4.7). To demonstrate that the best-fit solution to all seven samples is not strongly influenced by any single dataset, we also show in Fig. 2 that the solutions to each possible subset containing six samples (i.e., excluding each one of the 63503 datasets) are within the confidence interval of the best-fit solution.

To summarize, the duration and temperature of the hypothetical 3.3 Ga thermal event that best explain observed $(Dt/a^2)_k$ for all seven samples is $\sim 600^\circ\text{C}$ for $\sim 10^3\text{ s}$ (shown as the point in Fig. 2). The uncertainty analysis shows that days spent cooling back to surface temperatures is also permitted. This calculation shows that the entire dataset is well explained by a single and relatively short-duration heating event 3.3 Ga ago. As the samples are individual rocks, clearly there is some limit to how similar the thermal conditions experienced by each one 3.3 Ga ago can have been. However, it is clear that the thermal conditions permitted by the entire set of samples are more restricted than those permitted by any one sample. Note that violation of any of our assumptions would disrupt the observed concordance. In particular, protracted residence at low temperatures [e.g., due to recent solar heating at the Moon's surface (Turner, 1971)] is clearly excluded and would also cause a divergence in the initial step ages. The calculation also indicates that (i) the latest time of observable $^{40}\text{Ar}^*$ loss from these samples occurred ~ 3.3 Ga ago, and (ii) if multiple events affected these samples between 3.9 Ga and 3.3 Ga ago, the durations and temperatures of each event are constrained to be lower than the best-fit solution for a single event.

5.3. Physical conditions during the 3.3 Ga impact event

5.3.1. Constraints from the best-fit temperature and duration magnitude

Such a brief excursion to elevated temperatures limits the possible scenarios that could explain the observed $^{40}\text{Ar}^*$ distributions. A simple model for a hot sphere with the properties of typical geologic materials (thermal diffusivity $10^{-6}\text{ m}^2\text{ s}^{-1}$, specific heat $815\text{ J kg}^{-1}\text{ K}^{-1}$, density 2800 kg m^{-3}) cooling over hours from $\sim 600^\circ\text{C}$ to -20°C (mean near-surface temperature) in an infinite surrounding medium (Carslaw and Jaeger, 1959) would require that the sphere have a diameter of order of $\sim 0.1\text{ m}$. The confidence interval on the best-fit solution shown in Fig. 2 is consistent with heating times of seconds to days; a cooling time of ~ 10 days would imply a $\sim 5\text{ m}$ sphere. The diverse sources of particles in regolith 63500 and the likely mixing of regolith over 3.3 Ga are inconsistent with cooling of a single object of such small size. Therefore, $\sim 0.1\text{--}5\text{ m}$ more likely represents the effective length scale of thermal interaction between cold and hot material mixed rapidly during an impact. During impacts, melt may rapidly combine with shocked and un-shocked lithic clasts to form polymict breccias (Stöffler et al., 1985). Studies of a melt breccia boulder at Apollo 17 Station 6 revealed that cooling of such mixtures takes place in two phases: (i) initially very rapid cooling (as low as seconds) when cold clasts interact with hot melt, followed by (ii) much slower cooling after the entire mixture equilibrates (Simonds, 1975). We suggest an analogous scenario during the ~ 3.3 Ga impact recorded in 63503: a mixture of hot and cold clasts rapidly equilibrated and then cooled within hours to weeks. This scenario is consistent with the absence of 3.3 Ga plateau ages or significant quantities of 3.3 Ga-old melt.

To associate specific impact features on the Moon with geochronological data has proven to be remarkably difficult and has resulted in somewhat tenuous ages for the major impact basins (Maurer et al., 1978; Stöffler et al., 1985; Stadermann et al., 1991; Dalrymple and Ryder, 1993; Dalrymple and Ryder, 1996; Norman et al., 2006). As in the previous studies, the specific impact that produced the 3.3 Ga thermal event recorded in 63503 cannot be unambiguously determined. However, the fact that the impact did not completely reset $^{40}\text{Ar}/^{39}\text{Ar}$ plateau ages and was apparently not large enough to produce significant impact melt at the site does not strongly suggest a large basin-forming event. On the other hand, given that none of the 63503 samples records the North Ray Crater impact at 50 Ma (Schaeffer and Husain, 1973; Arvidson et al., 1975) suggests that the samples were not sensitive to small impacts ($\sim 1\text{ km}$) that produced relatively low temperature excursions. Turner et al. (1971) also found that an impact event ~ 26 Ma ago which resulted in the 300 m diameter Cone

Crater did not cause extensive diffusive loss of $^{40}\text{Ar}^*$ from Apollo 14 breccia fragments. Together, these observations suggest that the impact event recorded by the 63503 samples and impact events in general that result in partial resetting of the plagioclase K-Ar system are significantly larger than these relatively small impacts. A number of mapped Imbrian craters with diameters $>10\text{ km}$ surround the Apollo 16 site (Wilhelms and McCauley, 1971) and could be the source of the rocks, with the most likely candidates being Delamore (-1.9° , 17.5°E , 51 km diameter), Taylor (-5.3° , 6.7°E , 45 km), and Kant (-10.6° , 20.1°E , 33 km). Alternatively, the source may be a crater that has since been obliterated.

5.3.2. Constraints from cosmogenic $^{38}\text{Ar}/\text{Ca}$ ratios

Cosmic ray exposure (CRE) ages based on the ratio of cosmogenic ^{38}Ar ($^{38}\text{Ar}_{\text{cos}}$) to Ca-derived ^{37}Ar ($^{37}\text{Ar}_{\text{Ca}}$) [e.g., Levine et al., 2007; Turner et al., 1997] and assuming the ^{38}Ar production rate of (Eugster and Michel, 1995) are summarized in Table 2. With the exception of 63503,13, the apparent exposure ages indicate that the 63503 samples did not experience significant exposure to cosmic radiation, and so were not near the lunar surface, prior to excavation by the North Ray Crater event. Because ^{38}Ar is stable and could not have been lost by diffusion in the past 3.3 Ga without disturbing initial $^{40}\text{Ar}/^{39}\text{Ar}$ step ages, the remarkably low cosmogenic ^{38}Ar abundances require that all samples resided at least several tens of meters below the surface for nearly all of the duration between the 3.3 Ga impact event and their recent exposure $\sim 23\text{ Ma}$ or 50 Ma ago (Arvidson et al., 1975), although their positions relative to one another could have changed over this time interval (Russ, 1973; Russ et al., 1972). The consistency in $^{38}\text{Ar}_{\text{cos}}/^{37}\text{Ar}_{\text{Ca}}$ among the samples further suggests that the samples share a common history. All were most likely buried beneath a deep ejecta blanket between the 3.3 Ga impact event and recent excavation by the North Ray impact (which, based on these new data, appears to have occurred as recently as $\sim 23\text{ Ma}$ ago).

5.4. The possible influence of a non-uniform distribution of diffusive length scales

5.4.1. The single-domain assumption

Given that these are stepped-heating analyses of fragmented and multi-phase whole-rock samples, it is reasonable to question the assumption that a single apparent E_a and diffusive length scale (i.e., a) sufficiently parameterize the diffusive mobility and the ^{40}Ar spatial distributions within each sample. Indeed, the possibility of a distribution of diffusive length scales cannot be a priori excluded. If unrecognized, this condition would invalidate a primary assumption in the model used to calculate values of $\ln(D/a^2)$ from step release fractions (Fechtig and Kalbitzer, 1966). In particular, a distribution of

Table 2

Summary of cosmic ray exposure (CRE) ages.

Sample	$^{38}\text{Ar}_{\text{cos}}/^{37}\text{Ar}_{\text{Ca}}$ (mol/mol)	(+/-)	CRE age (Ma)	(+/-)
63503,1	0.00511	0.00017	27.0	0.9
63503,3	0.00461	0.00011	24.4	0.6
63503,4	0.00458	0.00016	24.2	0.9
63503,9a	0.00432	0.00012	22.8	0.7
63503,11	0.00508	0.00015	26.8	0.8
63503,13	0.03435	0.00065	181.7	3.4
63503,15	0.00457	0.00017	24.2	0.9

Errors are reported at the 1σ confidence level.

CRE ages are calculated using the following parameters:

$P_{38\text{Ca}} = 4.86 \times 10^{11}\text{ atoms/g-Ca/Ma}$; (Eugster and Michel, 1995).

We have neglected minor contributions of cosmogenic ^{38}Ar from K and heavier elements as their abundances in 63503 plagioclase are low.

$\gamma = 2.57 \times 10^{15}\text{ atoms/g-Ca}$; (Levine et al., 2007).

γ relates ^{37}Ar produced during neutron irradiation to the mass of Ca and is determined by irradiating a standard of known Ca concentration.

diffusive length scales would clearly manifest itself as (i) sequentially decreasing values of $\ln(D/a^2)$ calculated at a given temperature, which would result in a poorly fitting linear Arrhenius regression; and (ii) an erroneously low E_a calculated from the regression. This is simply because smaller domains (i.e., with smaller effective a) would more readily exhaust their ^{37}Ar and ^{39}Ar prior to larger grains.

We do not find strong statistical justification to exclude the single-domain Arrhenius relationships summarized in Table 1. The R^2 value of each linear regression is >0.98 , (including ≥ 12 points in each) and, in general, calculated values of $\ln(D/a^2)$ in isothermal steps are in good agreement. However, because (i) the χ^2_ν values for the linear regressions are >2 ; (ii) sequentially calculated values of $\ln(D/a^2)$ at constant temperature drop by more than analytical uncertainty in a few cases; and (iii) a distribution of diffusive length scales is clearly plausible given the nature of the samples, we cannot completely exclude the possibility that the values of E_a are somewhat influenced by a distribution of diffusive length scales. It is important to note that this would not strongly influence model calculations within the observed laboratory temperature interval (~ 370 – 1000 °C). However, it could potentially have a significant effect when calculations are extrapolated to lower and higher temperatures (i.e., as shown in Fig. 2).

5.4.2. A more complex model involving multiple diffusive length scales

To assess the possibility that the best-fit solution shown in Fig. 2 is biased by partial or complete failure in the single-domain model assumptions, in the following section we construct a more complex model in which material within each sample has invariant E_a but is permitted to display a range of diffusive length scales (i.e., variation in a). Because non-uniformity in a could lead to an underestimation in E_a in the single-domain model, our objective in adding model complexity is to place an upper bound on the permissible E_a for each sample. However, we do not have independent knowledge of either a more appropriate E_a or the actual domain size distribution within each sample. Even with accurate knowledge of the plagioclase size distributions (e.g., by physical measurement), observable grain geometries may not physically represent the limiting diffusive length scale in all cases [e.g., Lovera et al., 1997]. For these reasons, the more complex model described here involves a proliferation of new unknown parameters and is necessarily somewhat subjective.

A common approach in “multiple diffusion domain” (MDD) modeling of K-feldspar is to select the first few low- T steps that have replicate diffusivity during repeated extractions to quantify E_a , e.g., (Lovera et al., 1997) and then assert that (i) this E_a applies to higher- T steps, and (ii) the lower apparent E_a observed through higher- T steps is due to the admixture of prescribed proportions of gas in different domains having larger prescribed diffusive length scales (a). To place a reasonable maximum bound on the permissible E_a for a given sample, we also adopt this strategy in our multiple diffusive

length scale models (hereafter “MDD-type models”). In this case, this approach should therefore place an upper bound on duration and a corresponding lower bound on temperature of the late-stage heating event. Since it was recently demonstrated that individual crystals of terrestrial plagioclase do not always exhibit MDD behavior (Cassata et al., 2009), in the following discussion we explicitly use MDD-type models to investigate potential influence of non-uniform diffusion domain sizes within the 63503 whole-rock samples [i.e., Turner et al., 1966], rather than MDD behavior within individual plagioclase crystals.

Theoretical age spectra resulting from multiple diffusion domains subjected to a common $^{40}\text{Ar}^*$ loss event can be calculated in the same manner as those from a single diffusion domain, provided the E_a , D_0/a^2 , and relative concentration of ^{37}Ar , Φ , of each domain are either known or specified. For each of the seven analyses, the Ar release patterns are adequately predicted by four different domain sizes. Provided that the Arrhenius plot is adequately fit by the MDD model, it has been argued that the exact number of domains does not strongly influence the constrained thermal history (Lovera et al., 1991). We quantify E_a by linear regression to the first 2 to 5 low- T steps and assume that this E_a applies to all domains. Cassata et al. (2009) recently showed that individual plagioclase grains from a single terrestrial “hand sample” have different E_a . However, since the 63503 samples are fragmented pieces of once larger grains, the assumption of a common E_a is reasonable for the present calculation. We assign the fraction of ^{37}Ar within each of the four domains (Φ_i) by assuming that inflections on a plot of $\Sigma F^{37}\text{Ar}$ vs. the difference between the natural logarithm of a given D_0/a^2 value and that expected from the low-temperature Arrhenius relationship [i.e., $\ln(r/r_0)$] represent the sequential exhaustion of domains. We estimate D_0/a^2 for each domain by minimizing the error-weighted least-squares differences between the observed and predicted values of $\ln(D/a^2)$ (Table 3; Fig. S2). To summarize, these models (i) place an upper bound on the permissible E_a of each sample and (ii) encapsulate the possible influence of multiple diffusive length scales. However, they require six additional free parameters beyond the two required by the single-domain model.

For each sample, we used the diffusion kinetics and domain distributions listed in Table 3 and a numerical, forward ingrowth and diffusion model to predict $^{40}\text{Ar}/^{39}\text{Ar}$ spectra for the same thermal conditions as considered with the single-domain models (i.e., Figs. 1 and S1). The MDD-type models similarly constrain the temperature and duration combinations of the hypothetical heating event 3.3 Ga ago that are consistent with the observed $^{40}\text{Ar}/^{39}\text{Ar}$ age spectra. However, in this case the $^{40}\text{Ar}/^{39}\text{Ar}$ ratio of each simulated laboratory step is simply the sum of ^{40}Ar and ^{39}Ar contributions from all four domains (Fig. S2). As for diffusion from a single-domain, the best-fit model constrains the non-dimensional parameter Dt/a^2 and its uncertainty for each domain (Table 3; Fig. S2). Using Dt/a^2 of the largest domain $[(Dt/a^2)_4]$, we employed the same procedure outlined

Table 3

Summary of $^{40}\text{Ar}/^{39}\text{Ar}$ thermochronometry parameters for models involving multiple diffusive length scales.

Sample	E_a (kJ/mol)	$\ln(D_0/a^2)_1$ ($\ln(\text{s}^{-1})$)	Φ_1	$\ln(D_0/a^2)_2$ ($\ln(\text{s}^{-1})$)	Φ_2	$\ln(D_0/a^2)_3$ ($\ln(\text{s}^{-1})$)	Φ_3	$\ln(D_0/a^2)_4$ ($\ln(\text{s}^{-1})$)	Φ_4	n	χ^2_ν	$(Dt/a^2)_4$ ($\times 10^{-9}$)	(+)	(−)
63503,1	213.9	24.2	0.04	16.8	0.36	14.3	0.36	7.0	0.24	23	6.51	416.87	243.82	165.68
63503,3	218.7	24.5	0.03	17.5	0.20	13.9	0.48	13.3	0.29	20	6.86	17782.79	27926.02	14620.52
63503,4	267.8	29.8	0.06	24.4	0.11	20.9	0.38	14.0	0.45	17	2.89	3.72	1.65	1.14
63503,9a	223.6	24.0	0.02	17.0	0.16	11.2	0.40	8.6	0.43	21	7.27	1.66	7.67	1.65
63503,11	206.0	20.0	0.01	14.0	0.27	12.0	0.15	6.0	0.57	15	5.79	177.83	384.51	114.73
63503,13	196.8	21.0	0.02	13.2	0.29	9.6	0.47	9.2	0.22	21	3.34	89125.09	69364.23	44456.73
63503,15	194.9	21.3	0.05	15.7	0.12	12.0	0.46	7.0	0.37	21	8.11	501.19	390.06	250.00

Each sample is fit with a model containing four domains; each domain shares a common E_a , and Φ_i is the fraction of Ar contained within a given domain with $\ln(D_0/a^2)_i$.

The fit statistic (reduced chi-squared, χ^2_ν) corresponds to the Arrhenius model fits, which include n number of points.

The values of $(Dt/a^2)_4$ are quantified from the best-fitting agreement between a 3.3 Ga heating event model and the $^{40}\text{Ar}/^{39}\text{Ar}$ release data of each sample as determined from the minima in a fit statistic (also using χ^2_ν) calculated for various $(Dt/a^2)_4$ values as shown in S2.

$(Dt/a^2)_4$ corresponds to that of the largest domain.

The asymmetric errors in Dt/a^2 (+ and −) are estimated from the values calculated at fixed distances (typically $+1.2$ in χ^2_ν) above the best-fit solution.

in Section 5.2 to find the best-fit solution to all seven analyses (Figs. 3 and S3). However, each of the four domains would yield the same result as they are constrained to have the same E_a . Under the MDD-type model assumptions, the best-fit solution for the hypothetical 3.3 Ga event is $T \sim 300^\circ\text{C}$ for $t \sim 20$ yr (Fig. 3; minimum $\chi^2_v = 3.9$).

5.4.3. Physical implications of the MDD-type model results

The longer heating duration constrained by the MDD-type models implies sustained temperature elevation after any initial phase of rapid thermal equilibration between hot and cold rock, which was the process inferred to have produced rapid cooling in the single-domain model (Section 5.3.1). The energy source responsible for a more protracted heating event is most plausibly either an impact melt sheet or waste heat after shock compression. The cooling timescales for impact-generated melt sheets are often > 10 yr (Onorato et al., 1978), in agreement with the inferred cooling timescale. But the low temperatures suggest that all seven samples must have been far from any melt sheet, whose temperature would have exceeded $\sim 1000^\circ\text{C}$. If the energy source was waste heat from shock compression, the samples must have been beneath the transient cavity in order to be heated above 150°C [e.g., Turtle et al., 2003]. In either case, the spatial dimension of heating may relate to the crater size rather than a mixing length scale. A cooling timescale of 10–100 yr from 300°C implies length scales of 10–100 m, which are fairly small relative to the dimensions of many lunar craters. However, as argued previously in Section 5.3.1, even larger impacts such as Cone and North Ray Crater do not appear capable of partially resetting the plagioclase K–Ar system. Therefore, an alternative explanation is that the actual conditions experienced by the samples may be closer to the single-domain model solution (Fig. 3).

Regardless of the exact magnitude of the event, both the MDD-type and single-domain model solutions imply relatively brief and low-

intermediate-temperature processes that occur around impact craters. While some studies of low-temperature (100 – 600°C) impact processes exist (Trepmann et al., 2005), high-temperature melt products are more frequently studied, even though the volume of melt produced in a crater is relatively small. The common low-temperature histories of the 63503 samples may reflect not that the rocks were located in the same small region when they were heated ~ 3.3 Ga ago, but rather that the thermal alteration regime was associated with a characteristic mixing and heating process, in much the same way that completely melted rocks from craters of similar sizes might all have reasonably similar time-temperature histories.

5.4.4. Model comparison summary

Although the single-domain solution derived under the simplest set of assumptions effectively fits our observations (Fig. 2), we cannot completely exclude the possibility that these assumptions are too restrictive and the possibility that E_a is underestimated. In principle, a model containing more free parameters (such as the MDD-type models) should yield a better fit to observed $^{40}\text{Ar}/^{39}\text{Ar}$ spectra than one with fewer free parameters (the single-domain model). However, this is not systematically true in this case. The MDD-type models slightly improve the χ^2_v fit statistics of best-fit $^{40}\text{Ar}/^{39}\text{Ar}$ age spectra for most samples (compare the lower panels of Figs. S1 and S2). They significantly improve the Arrhenius plot χ^2_v fit statistics in some cases (e.g., 63503, 3, 4 and 15), but not in others (compare Tables 1 and 3). Thus, although the MDD-type models seem to be more physically plausible for the 63503 samples, they do not systematically perform better than the single-domain model. Because of this observation as well as the numerous additional assumptions required for the MDD-type models, we do not find strong evidence that the best-fit t – T solution inferred from the MDD-type models is more accurate than that inferred from the single-domain model.

Perhaps more importantly, however, the MDD-type models place an upper bound on the permissible E_a of each sample. In this particular case, this means the solution shown in Fig. S3 represents an upper bound on the duration magnitude (and corresponding lower bound on temperature) of the conditions 3.3 Ga ago. And due to the possibility that E_a may be underestimated in the single-domain models, the corresponding t – T solution (Figs. 2, 3) represents a strong lower bound on the duration magnitude (and corresponding upper bound on temperature). Therefore, the thermal conditions experienced by each sample 3.3 Ga ago most likely occur between these two “end-member” solutions (Fig. 3), which each appear to be reasonable and robust. Although estimating the scale of the event is sensitive to these differences, each end-member solution and all intervening conditions represent relatively brief durations of elevated temperature that are most likely associated with an impact event.

5.5. Lunar impacts recorded by partially reset $^{40}\text{Ar}/^{39}\text{Ar}$ ages of lunar samples

The fact that a single common impact ~ 3.3 Ga ago fully explains partially reset $^{40}\text{Ar}/^{39}\text{Ar}$ ages of multiple rocks from regolith 63503 demonstrates that $^{40}\text{Ar}/^{39}\text{Ar}$ thermochronometry of lunar samples has the potential to constrain the timing and magnitude of short-duration impact heating events. Many $^{40}\text{Ar}/^{39}\text{Ar}$ data from other Apollo 16 and 17 rocks also show clear evidence of late-stage partial $^{40}\text{Ar}^*$ loss (see Supplementary Table S2 and citations therein). If the partial $^{40}\text{Ar}^*$ loss generally reflects short-duration heating as we find for 63503, then these data contain information about lunar impacts over time and imply that plateau ages alone are an incomplete record of the impactor flux history recorded by the K–Ar system in lunar samples.

A compilation of initial step $^{40}\text{Ar}/^{39}\text{Ar}$ ages provides additional constraints on the impactor flux at the Moon’s surface which has not previously been considered. The additional data reveal overall decreasing numbers of observed impact ages after ~ 3.9 Ga, with

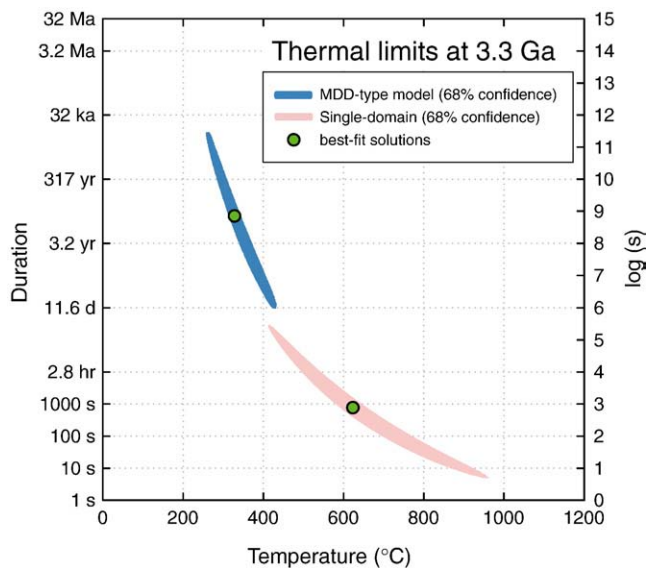


Fig. 3. Comparison between the best-fit solutions to the single-domain and MDD-type models. As in Fig. 2, the lower green point and the red ellipse are the best-fit solution and 68% confidence region calculated using single-domain diffusion models. The upper green point and the blue ellipse are the best-fit solution ($t \sim 20$ yr, $T \sim 300^\circ\text{C}$) and 68% confidence region calculated using the MDD-type models described in the text using parameters summarized in Table 3. The MDD Arrhenius plots and $^{40}\text{Ar}/^{39}\text{Ar}$ ratio evolution models for all seven samples appear in Fig. S2. Curves of constant Dt/a^2 for all seven samples used to calculate the best-fit MDD-type model solution appear in Fig. S3. Since the MDD-type models place an upper bound on the E_a of each sample, the corresponding best-fit solution places a lower bound on the temperature and upper bound on the duration of the 3.3 Ga heating event. The actual conditions experienced by the 63503 samples 3.3 Ga ago likely occur between these two end-member solutions.

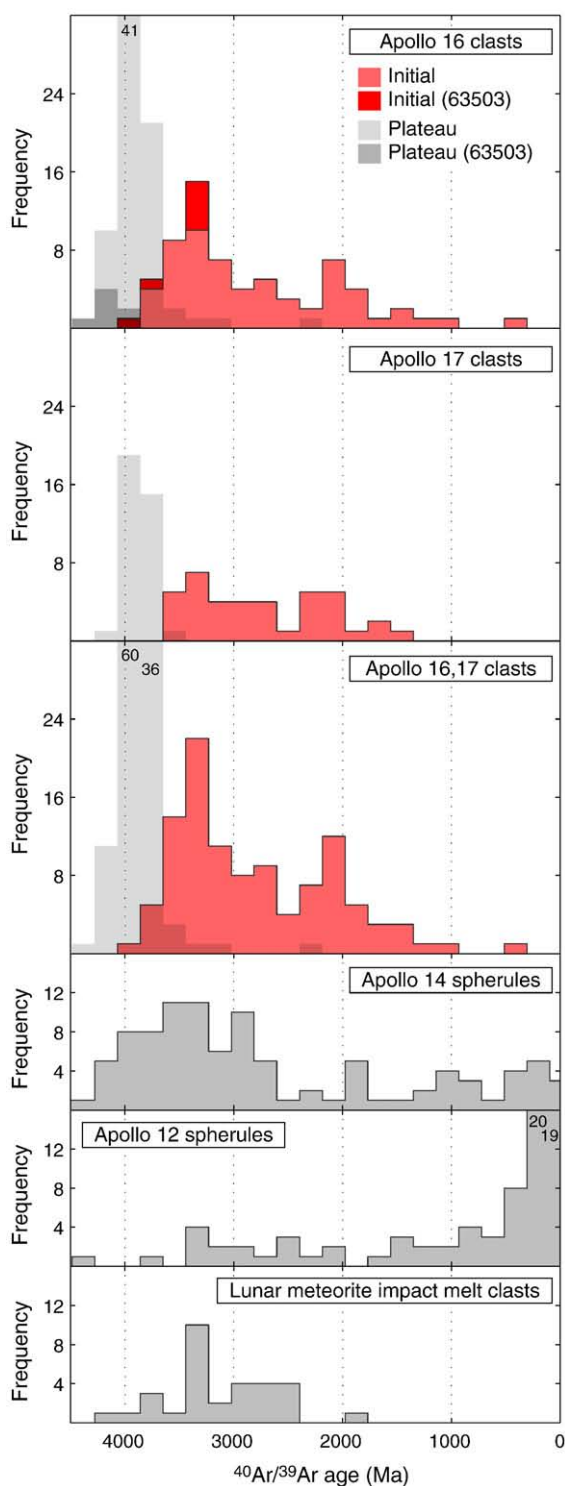


Fig. 4. Additional constraints on the Moon's impact history from partially reset $^{40}\text{Ar}/^{39}\text{Ar}$ ages of lunar rocks. Shown in light red and grey are the initial step ages, and $^{40}\text{Ar}/^{39}\text{Ar}$ plateau ages, respectively, of 123 published analyses of Apollo 16 and 17 rocks [see Supplementary Table S2; (Huneke et al., 1973; Schaeffer and Husain, 1973; Jessberger et al., 1974; Schaeffer and Husain, 1974; Maurer et al., 1978; Bernatowicz et al., 1986; Marvin et al., 1987; Dalrymple and Ryder, 1996; Norman et al., 2006)]. The initial step ages constrain the oldest apparent age of significant $^{40}\text{Ar}^*$ loss due to impact heating. The 63503 data highlighted in the upper panel are included in the third panel and summarized in Table 1. Shown for comparison in the bottom three panels are $^{40}\text{Ar}/^{39}\text{Ar}$ ages of 99 and 81 impact spherules from Apollo 14 and 12 regolith (Culler et al., 2000; Levine et al., 2005), respectively, as reported in Levine et al. (2005) and $^{40}\text{Ar}/^{39}\text{Ar}$ ages of 31 impact melt clasts from 4 different feldspathic lunar meteorites (Cohen et al., 2000; Cohen et al., 2005) reported in Cohen et al. (2005). All ages have been calculated using a common ^{40}K decay constant value (Supplementary Tables S1 and S2), and all data are shown in 200 Ma bins. Note that some bins extend off scale to the values shown in black.

almost none after 1.0 Ga (Fig. 4). Although we cannot directly relate published $^{40}\text{Ar}/^{39}\text{Ar}$ data from spatially unrelated samples to the single impact event recorded in 63503, many Apollo 16 and 17 samples show partially reset ages and some show plateau ages between ~ 3.2 and 3.4 Ga (Fig. 3). The fact that thermal disturbances are recorded ~ 3.3 Ga at both sites indicates either a relatively large impact or a number of smaller impacts near the time of partial resetting in 63503. While impacts smaller than those which produced the major impact basins are favored due to the incomplete resetting, high-resolution thermochronometry of other lunar samples would help distinguish these scenarios.

5.6. Comparison with other impact records

A variety of independent observations also record lunar impacts between ~ 3.2 and 3.4 Ga, including high abundances of ~ 3.2 to 3.4 Ga $^{40}\text{Ar}/^{39}\text{Ar}$ ages of lunar impact spherules from Apollo 12 and 14 (Culler et al., 2000; Levine et al., 2005) and lunar meteorites (Cohen et al., 2000; Cohen et al., 2005) (Fig. 4). Just as the age concordance of spatially unrelated samples helped identify an apparent episode of heavy bombardment ~ 3.9 Ga ago (Tera et al., 1974), so do these observations suggest that an episode of globally widespread yet perhaps smaller impacts occurred ~ 3.2 to 3.4 Ga ago, despite differences in the lithologies of these samples, their complex histories and any potential preservation bias (Hartmann, 2003). For example, many Apollo 12 and 14 lunar spherules have $^{40}\text{Ar}/^{39}\text{Ar}$ ages between 3.2 and 3.4 Ga, even though impact spherules may preferentially record relatively small events since 1.0 Ga ago (Levine et al., 2005) while the K-Ar systems of lunar surface rocks and meteorites do not (Fig. 4). The oldest impact-derived glass spherules in terrestrial samples, which may indirectly record impact events on Earth, also formed at around this time: the 3.24–3.26 Ga-old spherules in southwest Australia (Glikson and Vickers, 2006), and 3.40 Ga-old impact-generated silicate spherules observed in South Africa (Lowe and Byerly, 1986). A significant number of impact ages preserved in eucrites and howardites also occur in this time interval, suggestive of large impacts on the HED parent body as recently as ~ 3.4 Ga (Bogard, 1995).

Several high-resolution datasets from Apollo 16 and 17 (Dalrymple and Ryder, 1996; Norman et al., 2006) (Fig. 4), Apollo 15 samples (Ryder et al., 1991), and lunar meteorites (Haloda et al., 2009; Sokol et al., 2008) also record more recent episodes of $^{40}\text{Ar}^*$ loss between ~ 1.8 and 2.2 Ga ago, including the formation of the ~ 39 km diameter Autolycus impact structure on the Moon ~ 2.1 Ga ago (Ryder et al., 1991). The largest and oldest impact structures preserved on Earth formed in this time interval, including the ~ 300 km diameter Vredefort impact structure at 2.02 Ga (Moser, 1997) and the ~ 250 km Sudbury impact structure at 1.85 Ga (Krogh et al., 1984). As 63503 was collected near other Apollo 16 samples that experienced partial $^{40}\text{Ar}^*$ loss during this later period, our 63503 samples must have been insulated (presumably beneath the surface) from thermal events after ~ 3.3 Ga. Although the 63503 data preclude $^{40}\text{Ar}^*$ loss after 3.3 Ga, other nearby samples may record heating and $^{40}\text{Ar}^*$ loss both ~ 3.3 Ga and subsequently.

6. Conclusions

Our analysis of Apollo 16 sample 63503 demonstrates that partially reset $^{40}\text{Ar}/^{39}\text{Ar}$ ages of rocks in the lunar regolith can record impact events. Although previously unconsidered as a quantitative record, partially reset $^{40}\text{Ar}/^{39}\text{Ar}$ ages have been widely observed in other lunar rocks and provide additional constraints on the timing of lunar impacts at the Moon's surface. Taken together, these data suggest an overall declining impact frequency in the Solar System after 3.9 Ga, with a period of apparently high impactor flux between ~ 3.2 and 3.4 Ga and possibly between ~ 1.8 and 2.2 Ga. High impactor

fluxes in the inner Solar System at 3.9 Ga have been attributed to dynamical rearrangements in the outer Solar System (Dermott et al., 1991). The much more recent K/T boundary and Tycho crater impacts have also been explained by dynamical conditions in the asteroid belt object 160 Ma ago (Bottke et al., 2007). The episodic events observed in the lunar impact record over the last 4 Ga further demonstrate that strong pulses in the impactor flux may be common. These pulses may bias the photographically determined cratering record in some locations and have implications for conditions on Earth.

Acknowledgements

We thank the Apollo 16 team, the Johnson Space Center staff and the Curation and Analysis Planning Team for Extraterrestrial Samples for allocating the sample 63503 and T. Becker for the invaluable laboratory support and design of laser-heating hardware in collaboration with Photon Machines. This manuscript benefited from helpful discussions with F. Albarède, B. Kennedy, P. Renne, and G. Turner. The authors acknowledge O. Lovera, T. Harrison and an anonymous reviewer for their constructive comments on an earlier version of this manuscript. The authors acknowledge support from the NASA Lunar Advanced Science and Exploration Research Program, the NSF Major Research Instrumentation and Petrology and Geochemistry Programs, and the Ann and Gordon Getty Foundation. B.P.W. also thanks the NASA Lunar Science Institute and the Charles E. Reed Faculty Initiatives fund, and W.S.C. was supported by a NSF Graduate Research Fellowship.

Appendix A. Supplementary data

Supplementary data associated with this article can be found, in the online version, at doi: [10.1016/j.epsl.2009.12.016](https://doi.org/10.1016/j.epsl.2009.12.016).

References

- Albarède, F., 1978. The recovery of spatial isotope distributions from stepwise degassing data. *Earth Planet. Sci. Lett.* 39 (3), 387–397.
- Arvidson, R., Crozaz, G., Drozd, R.J., Hohenberg, C.M., Morgan, C.J., 1975. Cosmic ray exposure ages of features and events at the Apollo landing sites. *The Moon* 13, 259–276.
- Bernatowicz, T.J., Lindstrom, M.M., Podosek, F.A., 1986. ^{40}Ar – ^{39}Ar ages of Apollo 16 North Ray Crater Rocks and dimict breccias. *Proc. Lunar Sci. Conf.* 17, 42–43.
- Bevington, P.R., Robinson, D.R., 1992. *Data Reduction and Error Analysis for the Physical Sciences*. McGraw-Hill, New York.
- Bogard, D.D., 1995. Impact ages of meteorites – a synthesis. *Meteoritics* 30 (3), 244–268.
- Bottke, W.F., Vokrouhlicky, D., Nesvorný, D., 2007. An asteroid breakup 160 Myr ago as the probable source of the K/T impactor. *Nature* 449 (7158), 48–53.
- Carlsaw, H.S., Jaeger, J.C., 1959. *The Conduction of Heat in Solids*. Oxford University Press, London.
- Cassata, W.S., Renne, P.R., Shuster, D.L., 2009. Argon diffusion in plagioclase and implications for thermochronometry: a case study from the Bushveld Complex, South Africa. *Geochim. Cosmochim. Acta* 73, 660–6612.
- Cohen, B.A., Swindle, T.D., Kring, D.A., 2000. Support for the lunar cataclysm hypothesis from lunar meteorite impact melt ages. *Science* 290 (5497), 1754–1756.
- Cohen, B.A., Swindle, T.D., Kring, D.A., 2005. Geochemistry and ^{40}Ar – ^{39}Ar geochronology of impact-melt clasts in feldspathic lunar meteorites. Implications for Lunar Bombardment History, vol. 40(5, pp. 755–777.
- Culler, T.S., Becker, T.A., Muller, R.A., Renne, P.R., 2000. Lunar Impact History from ^{40}Ar – ^{39}Ar Dating of Glass Spherules. *Science*, vol. 287(5459), pp. 1785–1788.
- Dalrymple, G.B., Ryder, G., 1993. ^{40}Ar – ^{39}Ar ages of Apollo 15 impacts melt rocks by laser step heating and their bearing on the history of lunar basin formation. *J. Geophys. Res.* 98, 13085–13095.
- Dalrymple, G.B., Ryder, G., 1996. ^{40}Ar – ^{39}Ar age spectra of Apollo 17 highlands breccia samples by laser step heating and the age of the Serenitatis basin. *J. Geophys. Res.* 101 (E11), 26069–26084.
- Dermott, S.F., et al., 1991. The origin and evolution of the zodiacal dust cloud. *Lunar and Planetary Inst: Asteroids, Comets, Meteors*, pp. 153–156.
- Eugster, O., Michel, T., 1995. Common asteroid break-up events of eucrites, diogenites, and howardites and cosmic-ray production-rates for noble-gases in achondrites. *Geochim. Cosmochim. Acta* 59 (1), 177–199.
- Fechtig, H., Kalbitzer, S., 1966. The diffusion of argon in potassium bearing solids. In: Schaeffer, O.A., Zahringer, J. (Eds.), *Potassium–Argon Dating*. Springer, Heidelberg, pp. 68–106.
- Glikson, A., Vickers, J., 2006. The 3.26–3.24 Ga Barberton asteroid impact cluster: tests of tectonic and magmatic consequences, Pilbara Craton, Western Australia. *Earth Planet. Sci. Lett.* 241 (1–2), 11–20.
- Haloda, J., et al., 2009. Petrology, geochemistry, and age of low-Ti mare-basalt meteorite Northeast Africa 003-A: a possible member of the Apollo 15 mare basaltic suite. *Geochim. Cosmochim. Acta* 73, 3450–3470.
- Hartmann, W.K., 2003. Megaregolith evolution and cratering cataclysm models – lunar cataclysm as a misconception (28 years later). *Meteorit. Planet. Sci.* 38 (4), 579–593.
- Huneke, J.C., Jessberger, E.K., Podosek, F.A., Wasserburg, G.J., 1973. ^{40}Ar – ^{39}Ar measurements in Apollo 16 and 17 samples and the chronology of metamorphic and volcanic activity in the Taurus–Littrow region. *Proc. Lunar Sci. Conf.* 4 (2), 1725–1756.
- James, O.B., 1982. Petrologic and age relations of the Apollo 16 rocks – implications for subsurface geology and the age of the Nectaris basin. *Proc. Lunar Sci. Conf.* 12, 209–233.
- Jessberger, E.K., Huneke, J.C., Wasserburg, G.J., 1974. Evidence for A – 4.5 Aeon age of plagioclase clasts in a lunar highland breccia. *Nature* 248 (5445), 199–202.
- Jourdan, F., Renne, P.R., 2007. Age calibration of the Fish Canyon sanidine Ar-40/Ar-39 dating standard using primary K-Ar standards. *Geochim. Cosmochim. Acta* 71 (2), 387–402.
- Korotev, R.L., 1997. Some things we can infer about the Moon from the composition of the Apollo 16 regolith. *Meteorit. Planet. Sci.* 32 (4), 447–478.
- Krogh, T.E., Davis, D.W., Corfu, F., 1984. Precise U–Pb Zircon and Baddeleyite ages for the Sudbury area. In: Pye, E.G., Naldrett, A.J., Giblin, P.E. (Eds.), *The Geology and Ore Deposits of the Sudbury Structure: Ontario Geological Survey Special*, vol. 1, pp. 431–446.
- Lagarias, J.C., Reeds, J.A., Wright, M.H., Wright, P.E., 1998. Convergence properties of the Nelder–Mead simplex method in low dimensions. *Siam Journal on Optimization* 9 (1), 112–147.
- Levine, J., Becker, T.A., Muller, R.A., Renne, P.R., 2005. ^{40}Ar – ^{39}Ar Dating of Apollo 12 Impact Spherules. *Geophys. Res. Lett.*, vol. 32, no. 15: 4 pp.
- Levine, J., Renne, P.R., Muller, R.A., 2007. Solar and cosmogenic argon in dated lunar impact spherules. *Geochim. Cosmochim. Acta* 71 (6), 1624–1635.
- Levin, H.F., et al., 2009. Contamination of the asteroid belt by primordial trans-Neptunian objects. *Nature* 460 (7253), 364–366.
- Lovera, O.M., Grove, M., Harrison, T.M., Mahon, K.I., 1997. Systematic analysis of K-feldspar ^{40}Ar – ^{39}Ar step heating results: I. Significance of activation energy determinations. *Geochim. Cosmochim. Acta* 61 (15), 3171–3192.
- Lovera, O.M., Richter, F.M., Harrison, T.M., 1991. Diffusion domains determined by Ar-39 released during step heating. *Journal of Geophysical Research – Solid Earth and Planets* 96 (B2), 2057–2069.
- Lowe, D.R., Byerly, G.R., 1986. Early Archean silicate spherules of probable impact origin, South-Africa and Western Australia. *Geology* 14 (1), 83–86.
- Marvin, U.B., Lindstrom, M.M., Bernatowicz, T.J., Podosek, F.A., 1987. The composition and history of Breccia-67015 from North-Ray Crater. *Journal of Geophysical Research – Solid Earth and Planets* 92 (B4), E471–E490.
- Maurer, P., et al., 1978. Pre-Imbrian craters and basins – ages, compositions and excavation depths of Apollo 16 breccias. *Geochim. Cosmochim. Acta* 42, 1687–1720.
- McConville, P., Kelley, S., Turner, G., 1988. Laser probe Ar-40–Ar-39 studies of the Peace River shocked L6 chondrite. *Geochim. Cosmochim. Acta* 52 (10), 2487–2499.
- Moser, D.E., 1997. Dating the shock wave and thermal imprint of the giant Vredefort impact, South Africa. *Geology* 25 (1), 7–10.
- Nesvorný, D., Vokrouhlicky, D., Bottke, W.F., Gladman, B., Haggstrom, T., 2007. Express delivery of fossil meteorites from the inner asteroid belt to Sweden. *Icarus* 188 (2), 400–413.
- Neukum, G., Ivanov, B.A., Hartmann, W.K., 2001. Cratering records in the inner solar system in relation to the lunar reference system. *Space Science Reviews* 96, 55–86.
- Norman, M.D., Duncan, R.A., Huard, J.J., 2006. Identifying impact events within the lunar cataclysm from ^{40}Ar – ^{39}Ar ages and compositions of Apollo 16 impact melt rocks. *Geochim. Cosmochim. Acta* 70 (24), 6032–6049.
- Onorato, P.I.K., Uhlmann, D.R., Simonds, C.H., 1978. Thermal history of Manicouagan impact melt sheet, Quebec. *J. Geophys. Res.* 83 (NB6), 2789–2798.
- Reiners, P., 2009. Nonmonotonic thermal histories and contrasting kinetics of multiple thermochronometers. *Geochim. Cosmochim. Acta* 73 (12), 3612–3629.
- Russ, G.P., 1973. Apollo-16 neutron stratigraphy. *Earth Planet. Sci. Lett.* 19 (2), 275–289.
- Russ, G.P., G.J., Wasserburg, Burnett, D.S., 1972. Lunar neutron stratigraphy. *Earth Planet. Sci. Lett.* 15 (2), 172.
- Ryder, G., Bogard, D., Garrison, D., 1991. Probable age of Autolycus and calibration of lunar stratigraphy. *Geology* 19 (2), 143–146.
- Schaeffer, O.A., Husain, L., 1973. Early lunar history: ages of 2 to 4 mm soil fragments from the lunar highlands. *Proc. Lunar Sci. Conf.* 4, 1847–1863.
- Schaeffer, O.A., Husain, L., 1974. Chronology of lunar basin formation. *Proc. Lunar Sci. Conf.* 5, 1541–1555.
- Shuster, D.L., Weiss, B.P., 2005. Martian surface paleotemperatures from thermochronology of meteorites. *Science* 309 (5734), 594–597.
- Simonds, C.H., 1975. Thermal Regimes in Impact Melts and the Petrology of the Apollo 17 Station 6 Boulder. *Proc. Lunar Sci. Conf.* 6th, pp. 641–672.
- Sokol, A.K., et al., 2008. Geochemistry, petrology and ages of the lunar meteorites Kalahari 008 and 009: new constraints on early lunar evolution. *Geochim. Cosmochim. Acta* 72 (19), 4845–4873.
- Spudis, P.D., 1984. Apollo 16 site geology and impact melts: implications for the geologic history of the lunar highlands. *Proc. Lunar Sci. Conf.* 15, 95–107.
- Stadermann, F.J., Heusser, E., Jessberger, E.K., Lingner, S., Stoffler, D., 1991. The case for a younger Imbrium basin: new ^{40}Ar – ^{39}Ar ages of Apollo 14 rocks. *Geochim. Cosmochim. Acta* 55, 2339–2349.

- Stöffler, D., et al., 1985. Composition and evolution of the lunar crust in the Descartes highlands, Apollo 16. *Proc. Lunar Sci. Conf.* 15, 449–506.
- Stöffler, D., et al., 1982. Distribution and provenance of lunar highland rock types at North Ray Crater, Apollo 16. *Proc. Lunar Sci. Conf.* 12, 185–207.
- Stöffler, D., Ryder, G., 2001. Stratigraphy and isotope ages of lunar geologic units: chronological standard for the inner solar system. *Space Science Reviews* 96 (1–4), 9–54.
- Stöffler, D., et al., 2006. Reviews in mineralogy and geochemistry: cratering history and lunar chronology. *New Views of the Moon* 60, 519–596.
- Tera, F., Papanastasiou, D.A., Wasserburg, G.J., 1974. Isotopic evidence for a terminal lunar cataclysm. *Earth Planet. Sci. Lett.* 22 (1), 1–21.
- Trepmann, C.A., Gotte, T., Spray, J.G., 2005. Impact-related Ca-metasomatism in crystalline target-rocks from the Charlevoix structure, Quebec, Canada. *Can. Mineral.* 43, 553–567.
- Turner, G., 1971. ^{40}Ar – ^{39}Ar Ages from Lunar Maria. *Earth Planet. Sci. Lett.* 11 (3), 169–191.
- Turner, G., Huneke, J.C., Podosek, F.A., Wasserburg, G.J., 1972. ^{40}Ar – ^{39}Ar systematics in rocks and separated minerals from Apollo 14. *Lunar Science Conference*, 3rd, Houston, Texas, United States, pp. 1589–1612.
- Turner, G., 1979. Monte-Carlo model for the production of meteorites with implications for gas retention ages. *Meteoritics* 14 (4), 550–551.
- Turner, G., Huneke, J.C., Podosek, F.A., Wasserburg, G.J., 1971. ^{40}Ar – ^{39}Ar ages and cosmic-ray exposure ages of Apollo-14 samples. *Earth Planet. Sci. Lett.* 12 (1), 19–35.
- Turner, G., Knott, S.F., Ash, R.D., Gilmour, J.D., 1997. Ar–Ar chronology of the Martian meteorite ALH84001: evidence for the timing of the early bombardment of Mars. *Geochim. Cosmochim. Acta* 61 (18), 3835–3850.
- Turner, G., Miller, J.A. and Grasty, R.L., 1966. The thermal history of the Bruderheim meteorite. *Earth Planet. Sci. Lett.* 10.1016/0012-821X(66)90061-6.
- Turtle, E.P., Pierazzo, E., O'Brien, D.P., 2003. Numerical modeling of impact heating and cooling of the Vredefort impact structure. *Meteorit. Planet. Sci.* 38 (2), 293–303.
- Ulrich, G.E., Hodges, C.A., Muehlberger, W.R., 1981. *Geology of the Apollo 16 Area, Central Lunar Highlands*. USGS Professional Paper 1048, Washington.
- Wilhelms, D.E., 1987. *Geologic History of the Moon*. USGS Professional Paper 1348.
- Wilhelms, D.E., McCauley, J.F., 1971. *Geologic Map of the Near Side of the Moon*. USGS Map I-703.

Supplementary Files for:

A record of impacts preserved in the lunar regolith

David L. Shuster^{1*}, Greg Balco^{1,2,a}, William S. Cassata^{1,2,a}, Vera A. Fernandes^{1,2,a}, Ian Garrick-Bethell^{3,a,b}, Benjamin P. Weiss^{3,a}

¹Berkeley Geochronology Center, 2455 Ridge Road, Berkeley, CA 94709, USA

²Department of Earth and Planetary Sciences, University of California - Berkeley, 307 McCone Hall, Berkeley, CA 94720-4767, USA

³Department of Earth, Atmospheric and Planetary Sciences, Massachusetts Institute of Technology, 77 Massachusetts Avenue, Cambridge, MA 02139, USA

^aAuthors listed alphabetically.

^bNow at Department of Geological Sciences, Brown University, 324 Brook Street, Box 1846, Providence, RI 02912.

*To whom correspondence should be addressed. E-mail: dshuster@bgc.org

Contents:

Supplementary Figures

Fig. S1. Data and single-domain models for all 7 samples.

Fig. S2. Data and multiple-domain models for all 7 samples.

Fig. S3. Constraints on the 3.3 Ga thermal event from the multiple-domain models.

Supplementary Tables

Table S1. Complete $^{40}\text{Ar}/^{39}\text{Ar}$ incremental heating results.

Table S2. Summary of representative published Apollo 16 and 17 $^{40}\text{Ar}/^{39}\text{Ar}$ datasets.

Supplementary Figure Captions

Shuster et al., 2009

Fig. S1. Single-domain models. $^{40}\text{Ar}/^{39}\text{Ar}$ thermochronometry for seven individual rocks from Apollo 16 regolith samples: 63503,1 (**S1a**), 63503,3 (**S1b**), 63503,4 (**S1c**), 63503, 9a (**S1d**), 63503,11 (**S1e**), 63503,13 (**S1f**), and 63503,15 (**S1g**). (**Top Panels**) Diffusivity as a function of temperature (Arrhenius plot) calculated from ^{37}Ar data. Points are diffusion coefficients calculated (Fechtig and Kalbitzer, 1966) using measured ^{39}Ar (circles) and ^{37}Ar (triangles) release fractions. Because ^{37}Ar release fractions yield slightly more linear Arrhenius relationships with less scatter than ^{39}Ar , we use the higher-precision ^{37}Ar -based diffusion kinetics in our models (Table 1). The lines are the model $D(T)/a^2$ obtained from the linear regressions to ^{37}Ar data collected below 900°C (above which point an apparent phase transition occurs in plagioclase) and used to calculate the curves shown in **Middle Panels**, for each sub-sample. $D(T)$ is the diffusivity of Ar as a function of temperature T and a is the radius of the model diffusion domain. (**Middle Panels**) Measured and modeled $^{40}\text{Ar}^*/^{39}\text{Ar}$ ratio evolution spectra. $^{40}\text{Ar}^*$ represents radiogenic ^{40}Ar , corrected for blank, mass discrimination and reactor-produced interferences to the measured ^{40}Ar signals (Table S1). Circles are the measured $^{40}\text{Ar}^*/^{39}\text{Ar}$ ratios (R) normalized to the mean ratio of the plateau (R_{plateau}) with associated uncertainties plotted versus the cumulative ^{39}Ar release fraction ($\Sigma F^{39}\text{Ar}$). Also shown as curves are modeled release spectra using a spherical, one-domain model for heating at 3.3 Ga lasting 1 hour from the present mean lunar surface temperature (-25°C) to various constant temperatures. These models correspond to specific values of Dt/a^2 shown in **Lower Panels**. (**Lower Panels**) The reduced chi squared (χ_v^2) fit statistics for various model heating events at 3.3 Ga plotted versus values of $\log(Dt/a^2)$. The best-fit value of Dt/a^2 for each sample is identified at the minimum in χ_v^2 ; colored points correspond to temperatures shown **Middle Panels**. Uncertainty in the value of Dt/a^2 for each sample is estimated from the two values of Dt/a^2 located at a distance of $+1.2$ in χ_v^2 units above the best fit value. The grey values shown in Fig. S1b were calculated using the entire dataset, whereas the black values were calculated for $\Sigma F^{37}\text{Ar}$ up to ~ 0.6 . In each case, the best-fit value of Dt/a^2 is nearly equivalent.

Fig. S2. Multiple-domain models. $^{40}\text{Ar}/^{39}\text{Ar}$ thermochronometry for seven individual rocks from Apollo 16 regolith samples: 63503,1 (**S2a**), 63503,3 (**S2b**), 63503,4 (**S2c**), 63503, 9a (**S2d**), 63503,11 (**S2e**), 63503,13 (**S2f**), and 63503,15 (**S2g**). (**Top Panels**) Diffusivity as a function of temperature (Arrhenius plot) calculated from ^{37}Ar data. Triangles are diffusion coefficients calculated (Fechtig and Kalbitzer, 1966) using measured ^{37}Ar release fractions. The black line is a linear regression to the lowest temperature steps to estimate the upper bound on E_a for the MDD-type model. The blue diamonds and blue lines represent the multiple-domain model fit to the ^{37}Ar -based diffusion coefficients using the 4 specified domain sizes and gas fractions listed in Table 2. This MDD-type model and corresponding parameters are used to calculate the colored release patterns shown in **Middle Panels** for each sub-sample. $D(T)$ is the diffusivity of Ar as a function of temperature T and a is the radius of the model diffusion domain. (**Middle Panels**) Measured and modeled $^{40}\text{Ar}^*/^{39}\text{Ar}$ ratio evolution spectra. $^{40}\text{Ar}^*$

represents radiogenic ^{40}Ar , corrected for blank, mass discrimination and reactor-produced interferences to the measured ^{40}Ar signals (Table S1). Circles are the measured $^{40}\text{Ar}^*/^{39}\text{Ar}$ ratios (R) normalized to the mean ratio of the plateau (R_{plateau}) with associated uncertainties plotted versus the cumulative ^{39}Ar release fraction ($\Sigma F^{39}\text{Ar}$). Also shown as “stair step” patterns are modeled release spectra using the MDD-type model for heating at 3.3 Ga lasting 1 hour from the present mean lunar surface temperature (-25°C) to various constant temperatures. The MDD-type models are calculated solely for steps at which extraction temperature was accurately measured. These models correspond to specific values of Dt/a^2 for each domain size; for comparison we show the corresponding values for the largest domain size $(Dt/a^2)_4$ in each model in the **Lower Panels**. (**Lower Panels**) The reduced chi squared (χ_v^2) fit statistics for various model heating events at 3.3 Ga plotted versus values of $\log[(Dt/a^2)_4]$. The fit statistic is calculated solely for steps at which the MDD-type model is calculated as shown in **Middle Panels**. The best-fit value of $(Dt/a^2)_4$ for each sample is identified at the minimum in χ_v^2 ; colored points correspond to temperatures shown **Middle Panels**. Uncertainty in the value of $(Dt/a^2)_4$ for each sample is estimated from the two values of $(Dt/a^2)_4$ located at a distance of $+1.2$ in χ_v^2 units above the best fit value.

Fig. S3. Time-temperature constraints on a thermal excursion experienced by 63503 at 3.3 Ga from the MDD-type models. The constraint is derived from the entire $^{40}\text{Ar}^*/^{39}\text{Ar}$ dataset of seven rocks from sample 63503. The solution set of t - T combinations shown as curves of constant Dt/a^2 were constrained by independently observed $^{40}\text{Ar}/^{39}\text{Ar}$ age spectra and MDD-type diffusion models summarized in Table 2 of the seven sub-samples (Fig. S2). Each curve indicates the time (duration) and temperature combinations at 3.3 Ga which result in the observed $^{40}\text{Ar}/^{39}\text{Ar}$ spectrum of each rock. The green point is the best-fit solution to all seven ($t \sim 23$ yr, $T \sim 330^\circ\text{C}$). The 68% confidence region on this solution is shown as a red ellipse (see Methods). The blue points are solutions calculated from each of the subsets including only 6 samples. These solutions demonstrate that the best-fit solution is not strongly influenced by any one particular dataset, with perhaps the exception of 63503,4 in this case.

References

Fechtig, H. and Kalbitzer, S., 1966. The diffusion of argon in potassium bearing solids. In: O.A. Schaeffer and J. Zahringer (Editors), Potassium-Argon Dating. Springer, Heidelberg, pp. 68-106.

Figure S1a
Shuster et al., 2009

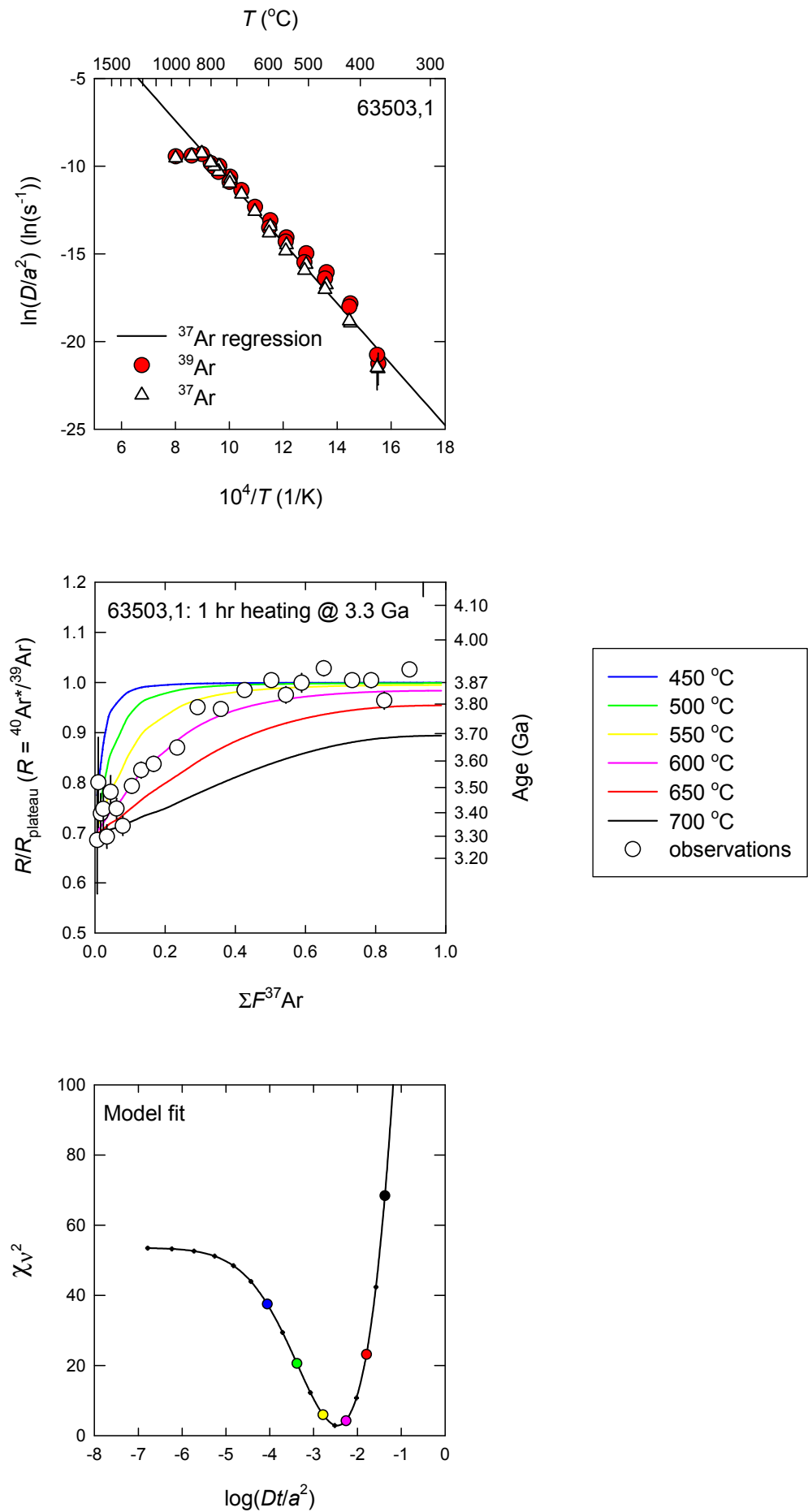


Figure S1b
Shuster et al., 2009

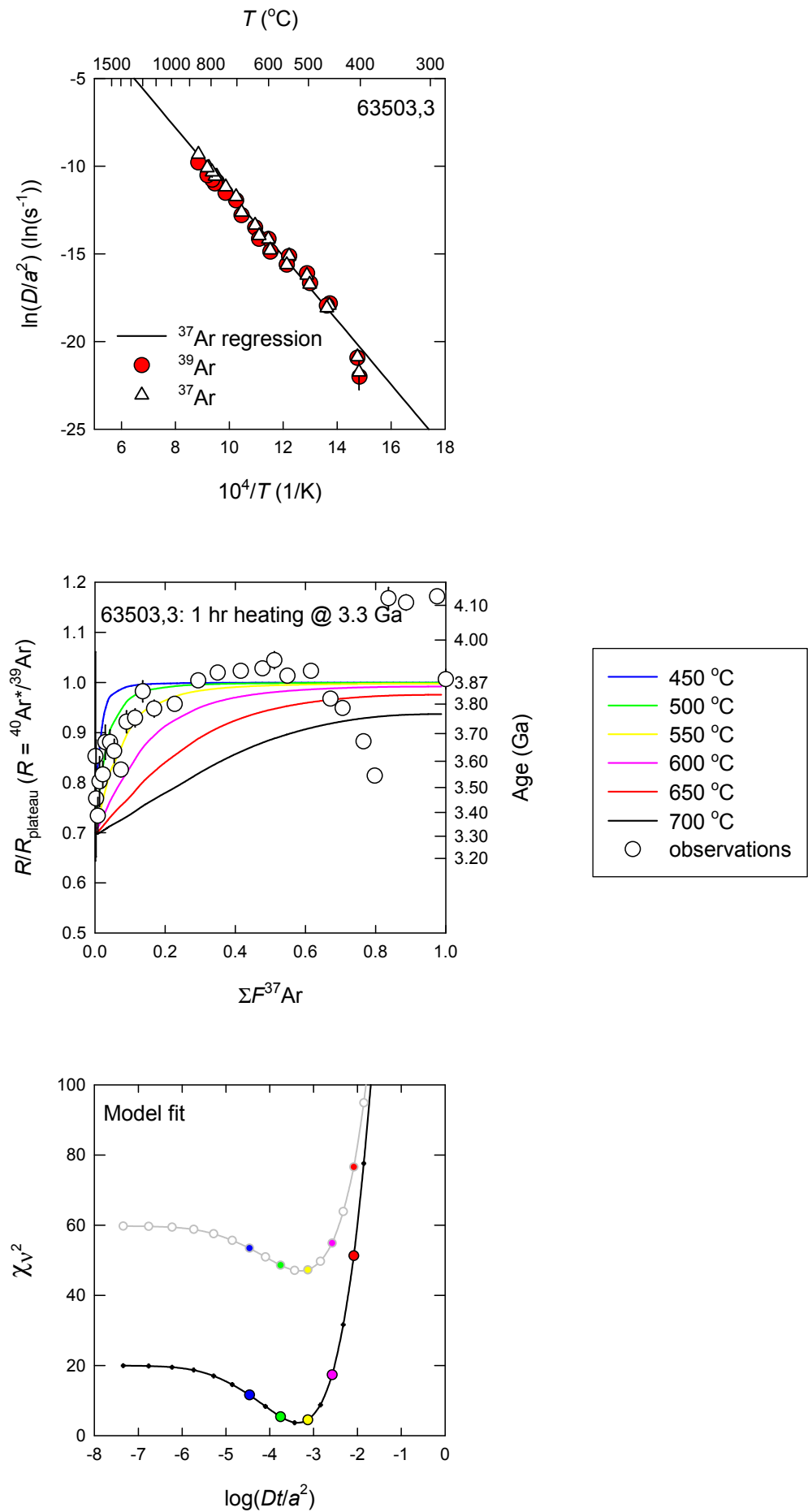


Figure S1c
Shuster et al., 2009

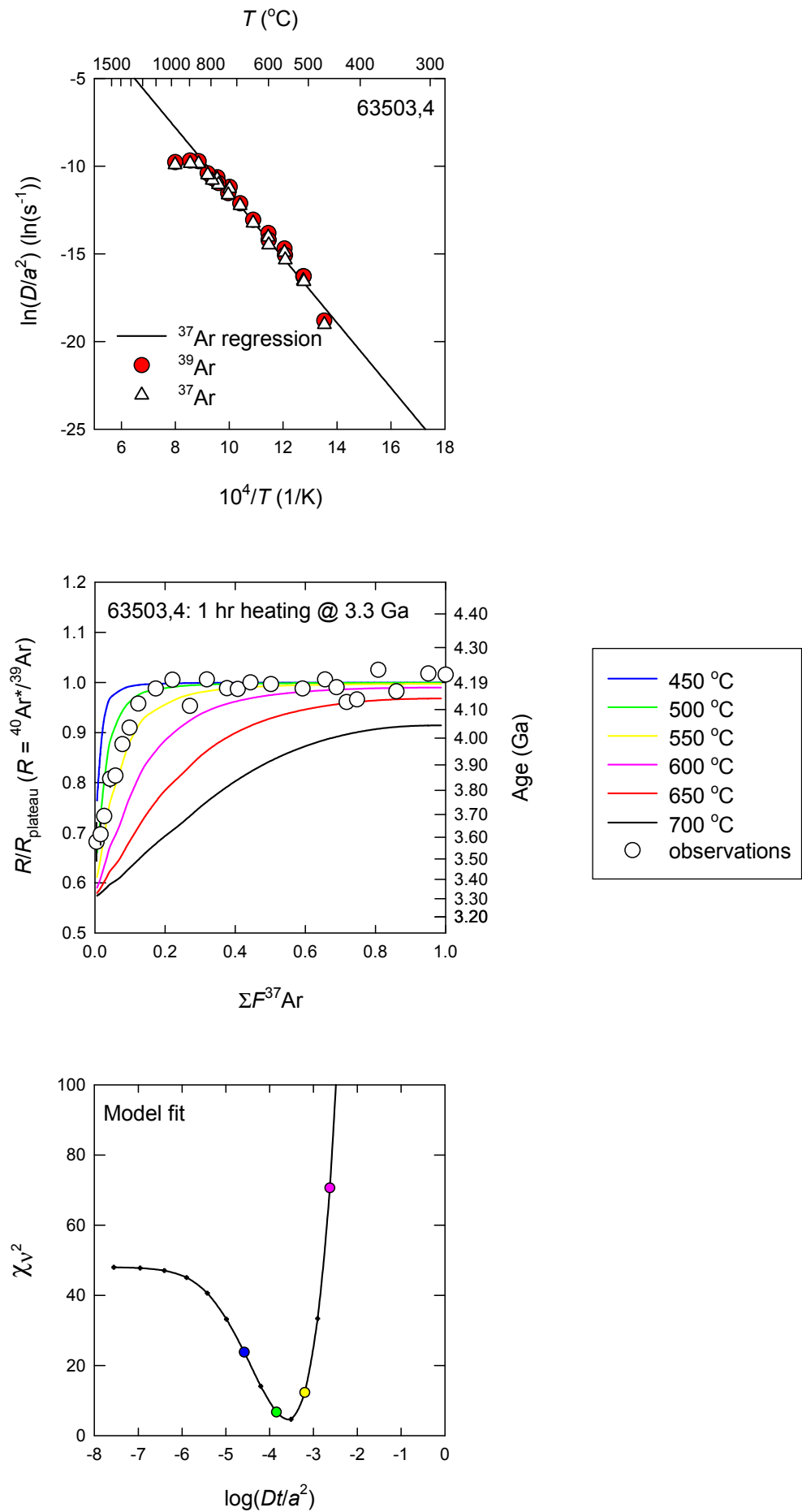


Figure S1d
Shuster et al., 2009

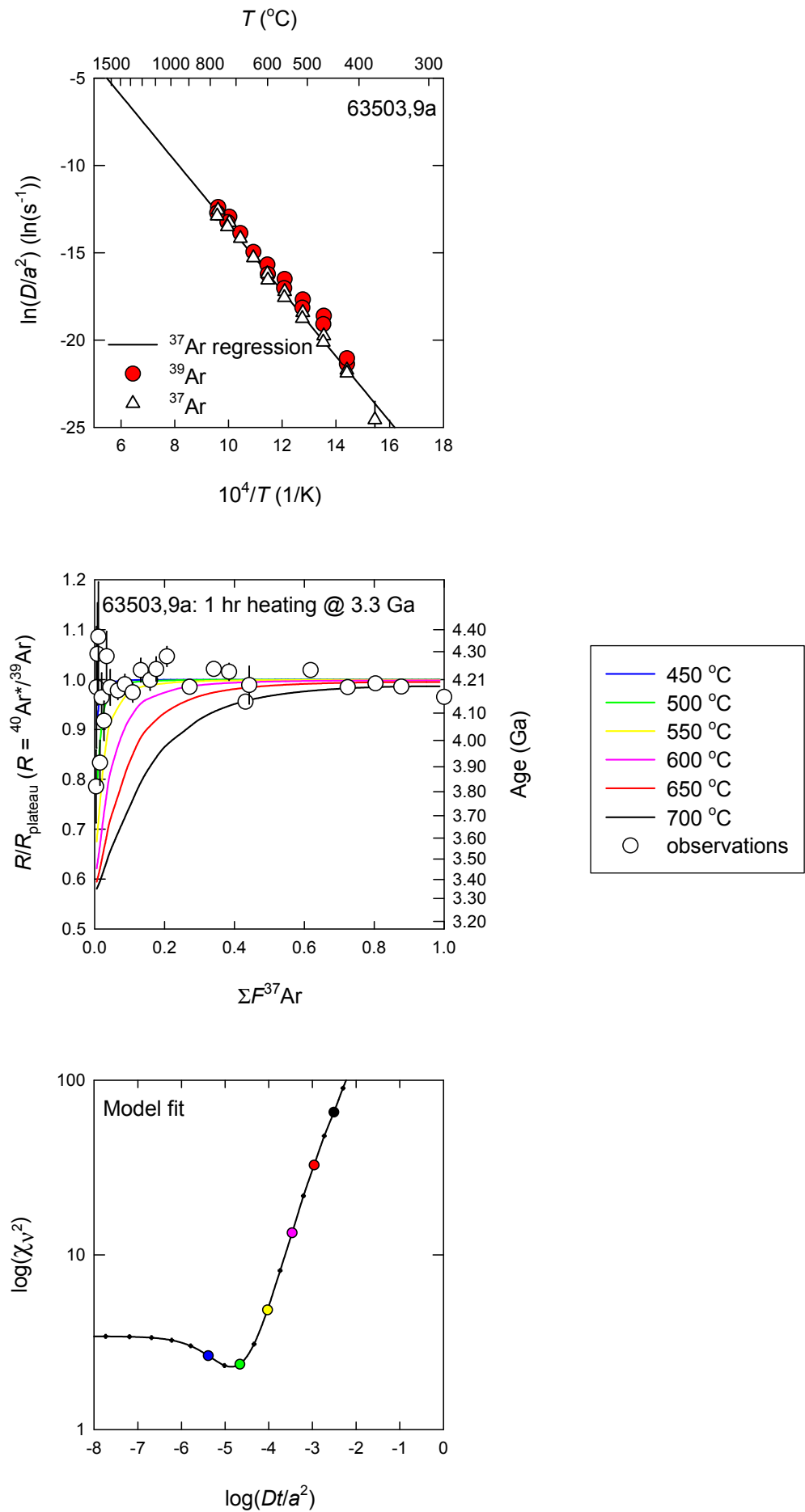


Figure S1e
Shuster et al., 2009

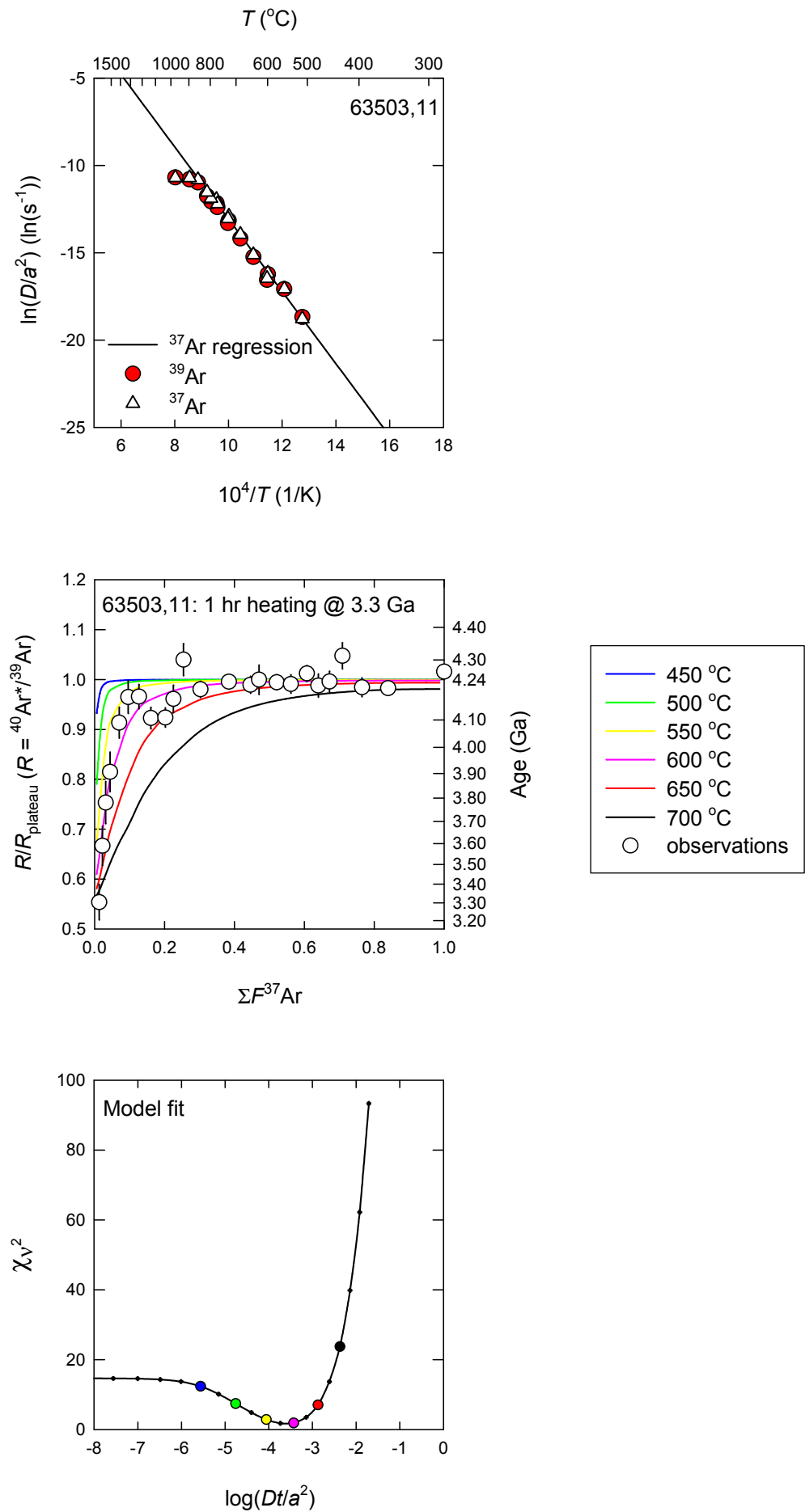


Figure S1f
Shuster et al., 2009

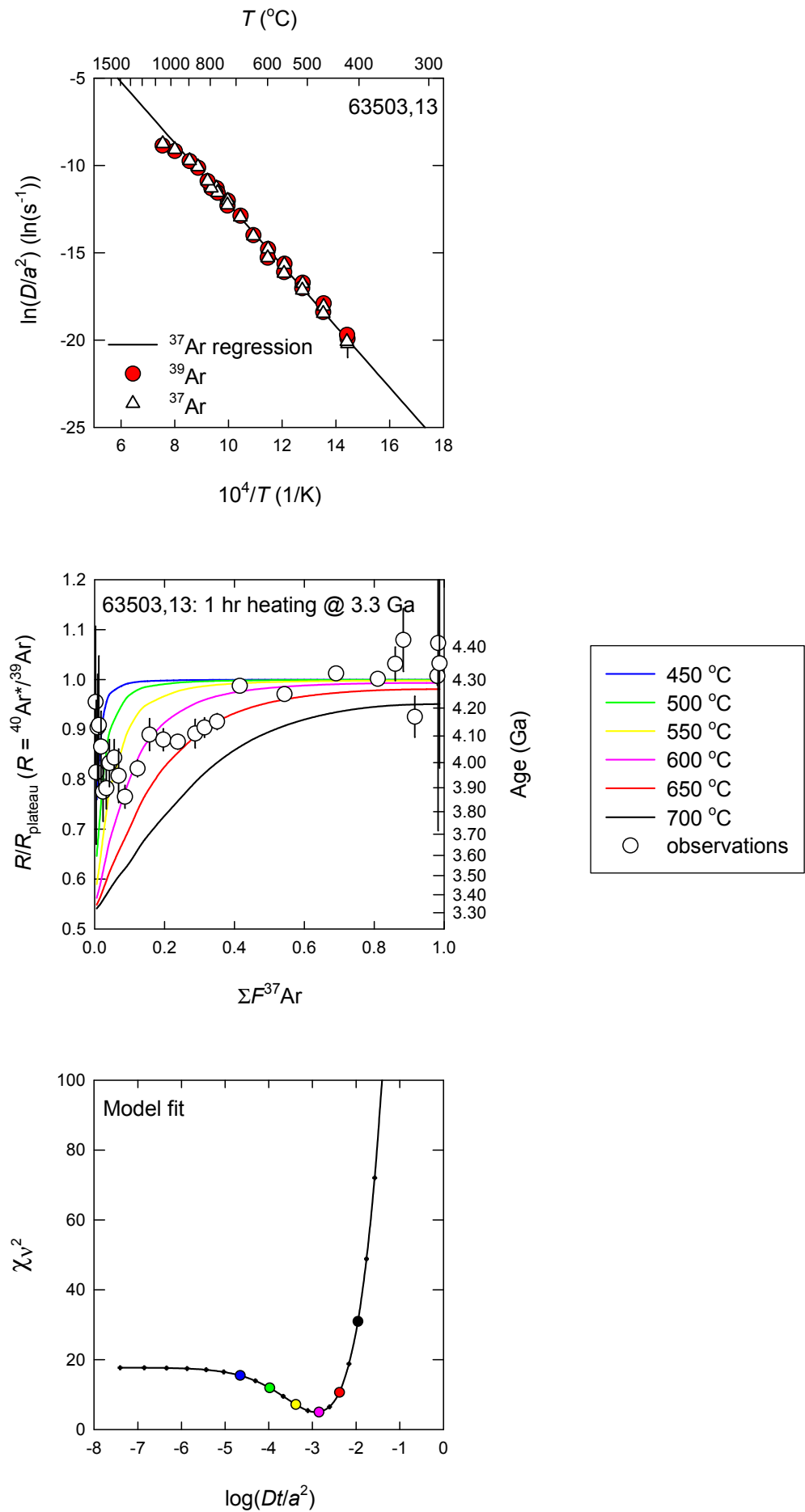


Figure S1g
Shuster et al., 2009

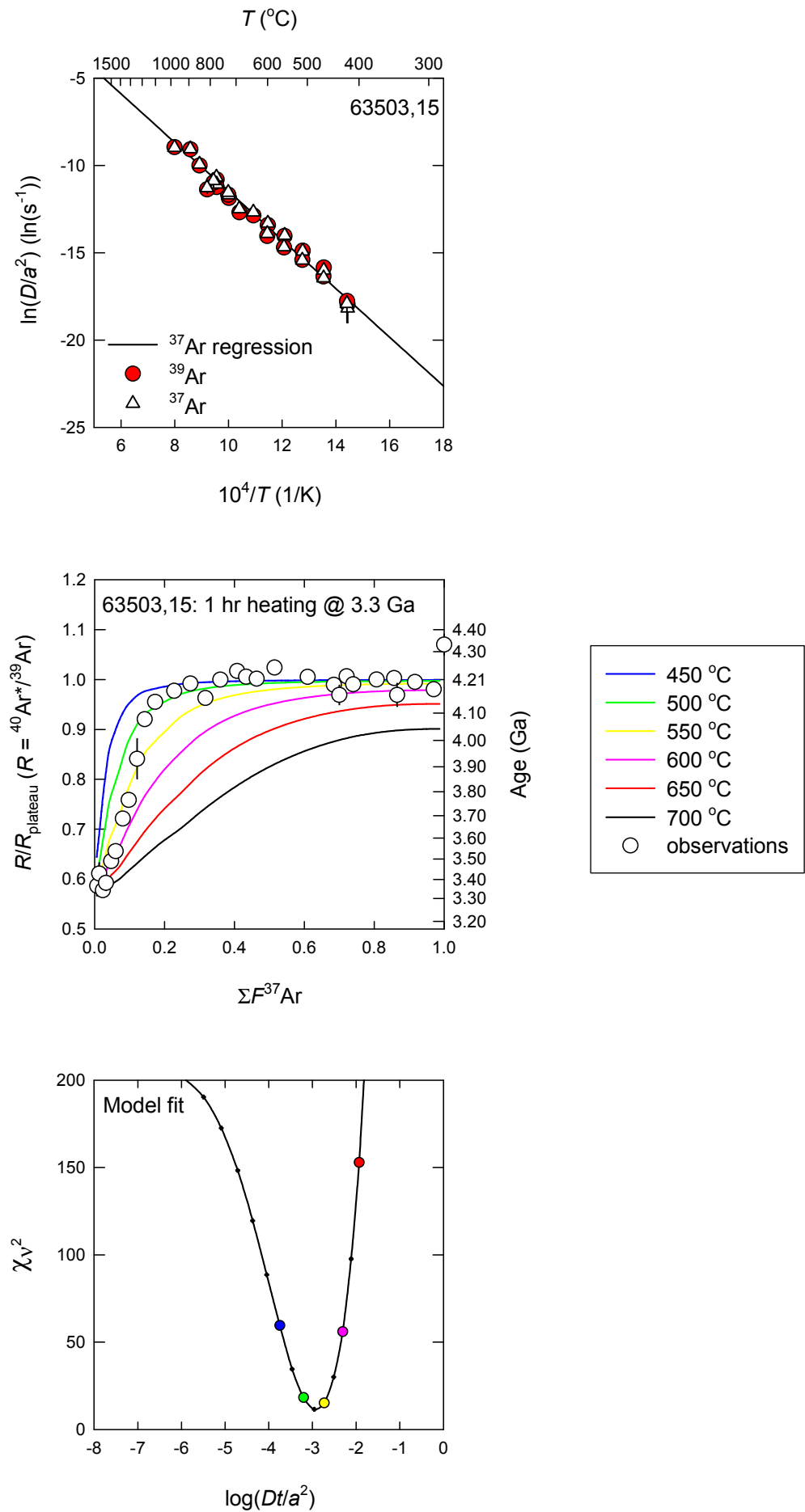


Figure S2a
Shuster et al., 2009

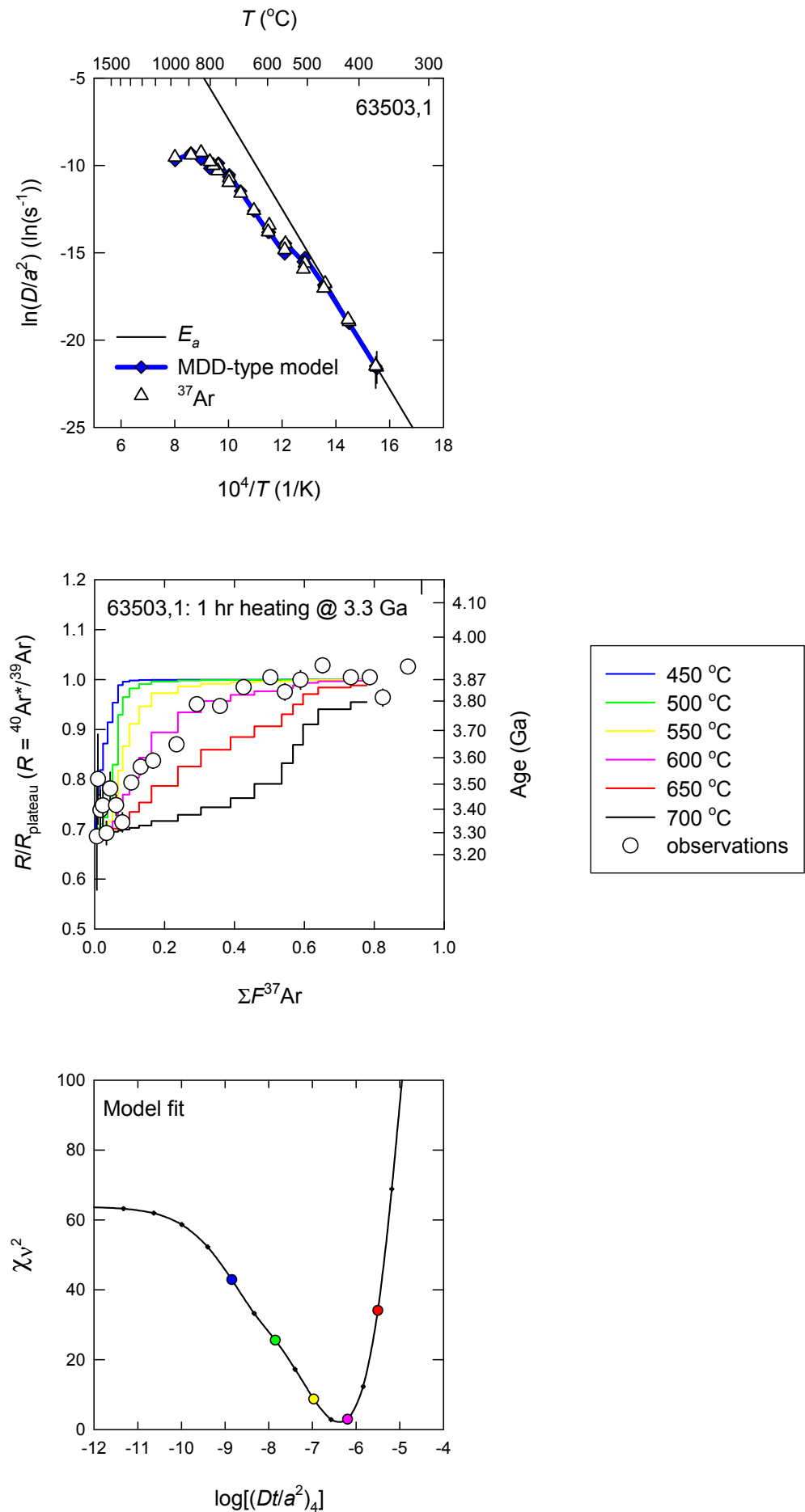


Figure S2b
Shuster et al., 2009

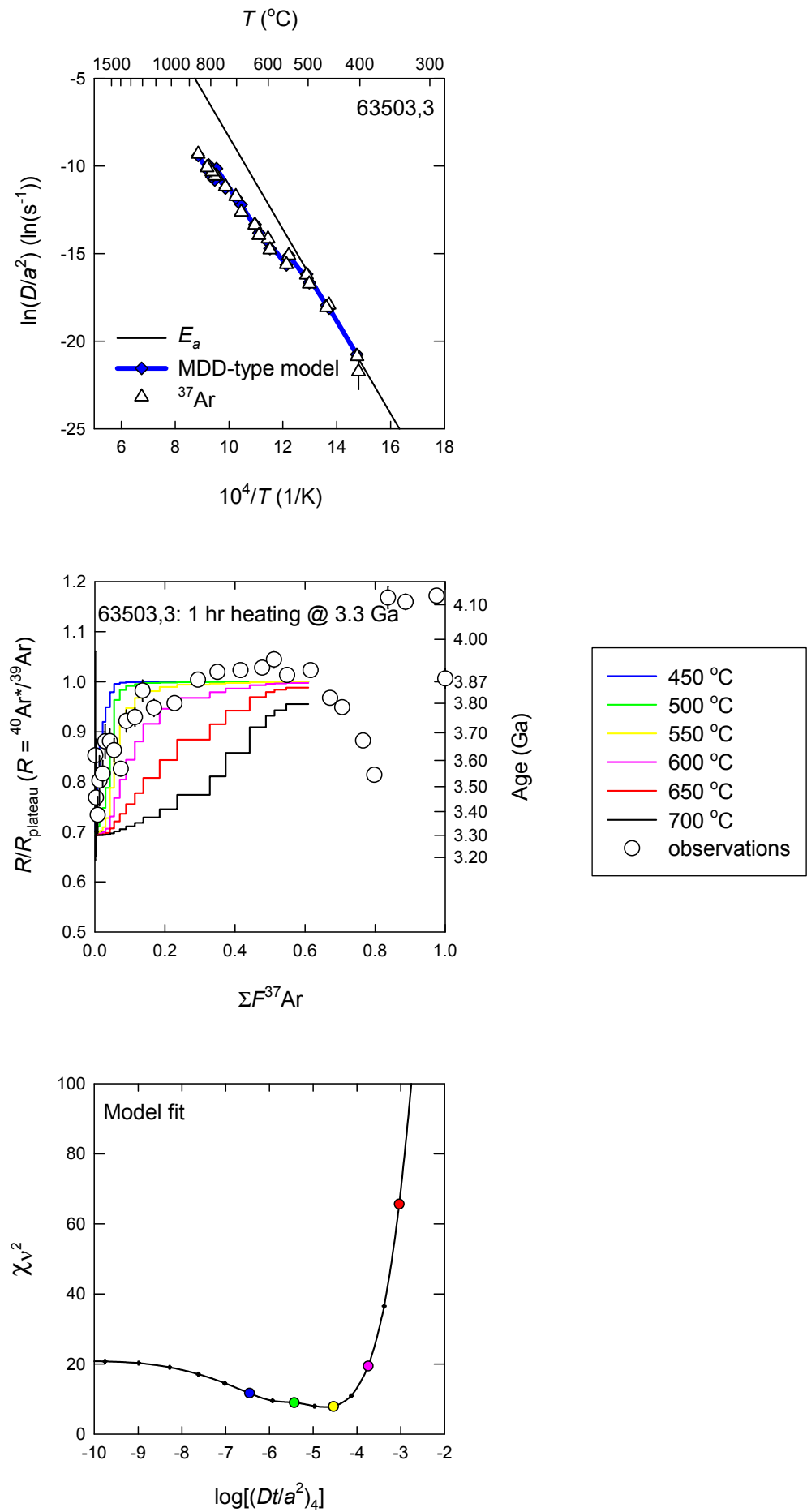


Figure S2c
Shuster et al., 2009

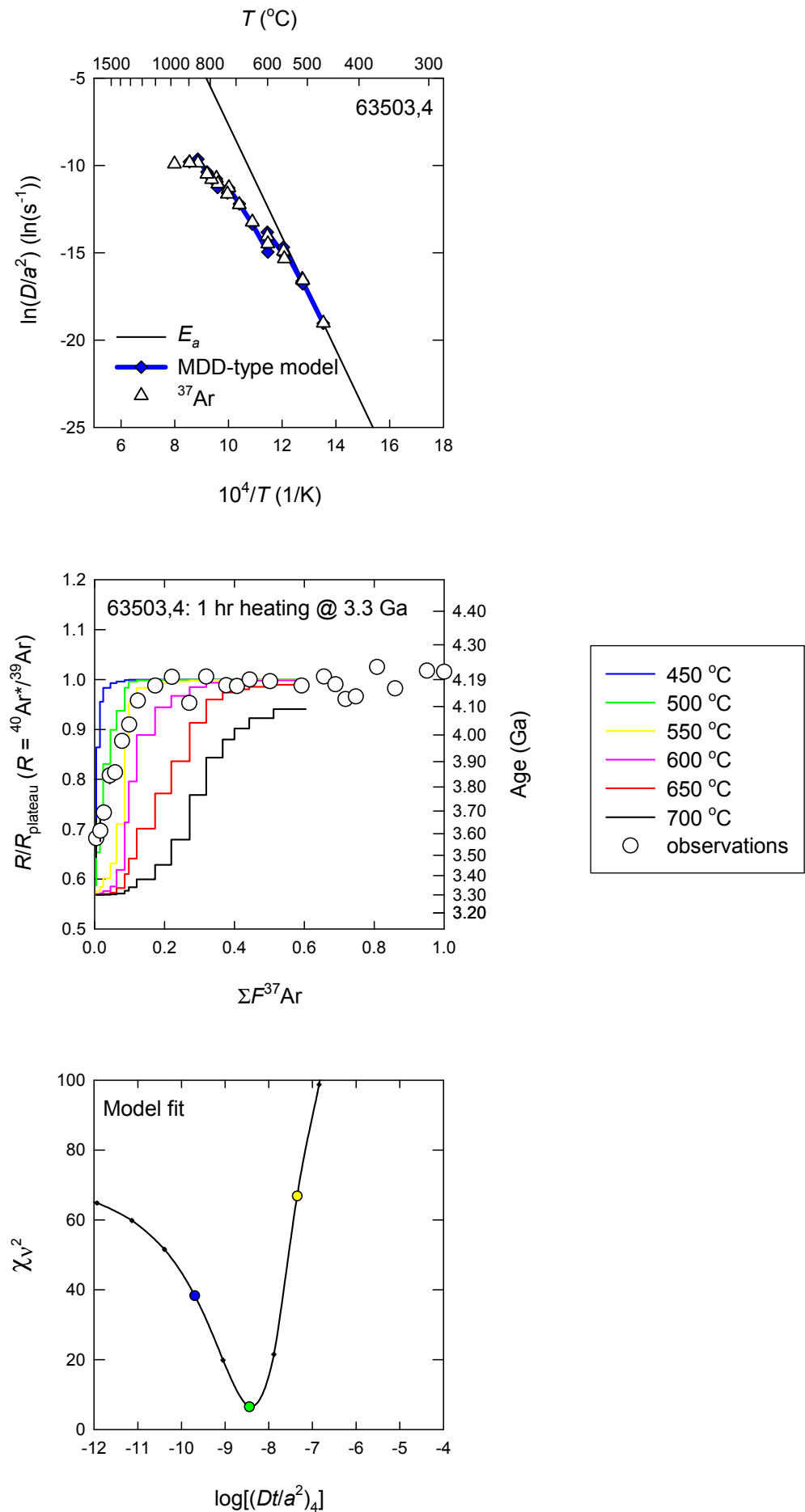


Figure S2d
Shuster et al., 2009

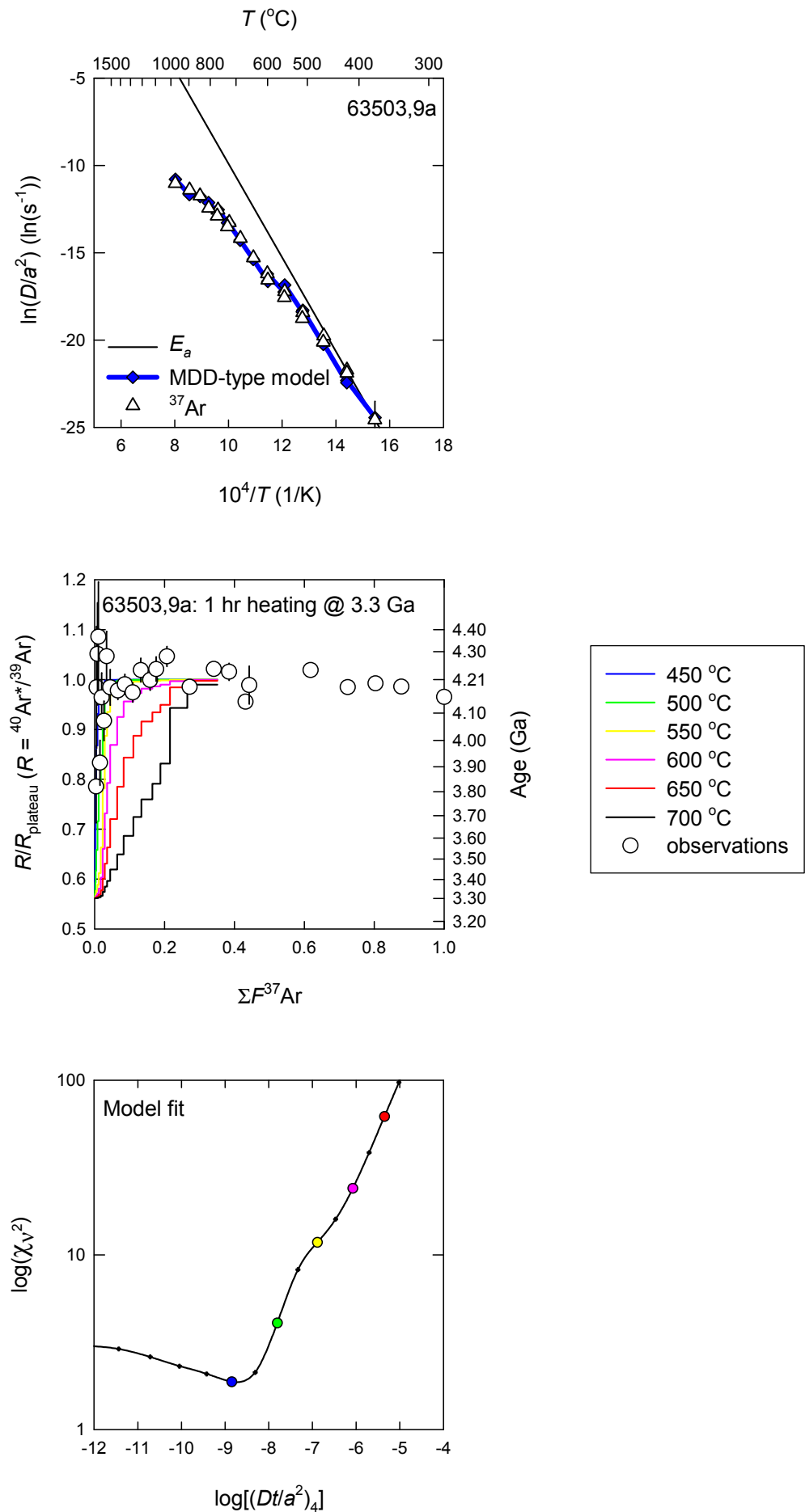


Figure S2e
Shuster et al., 2009

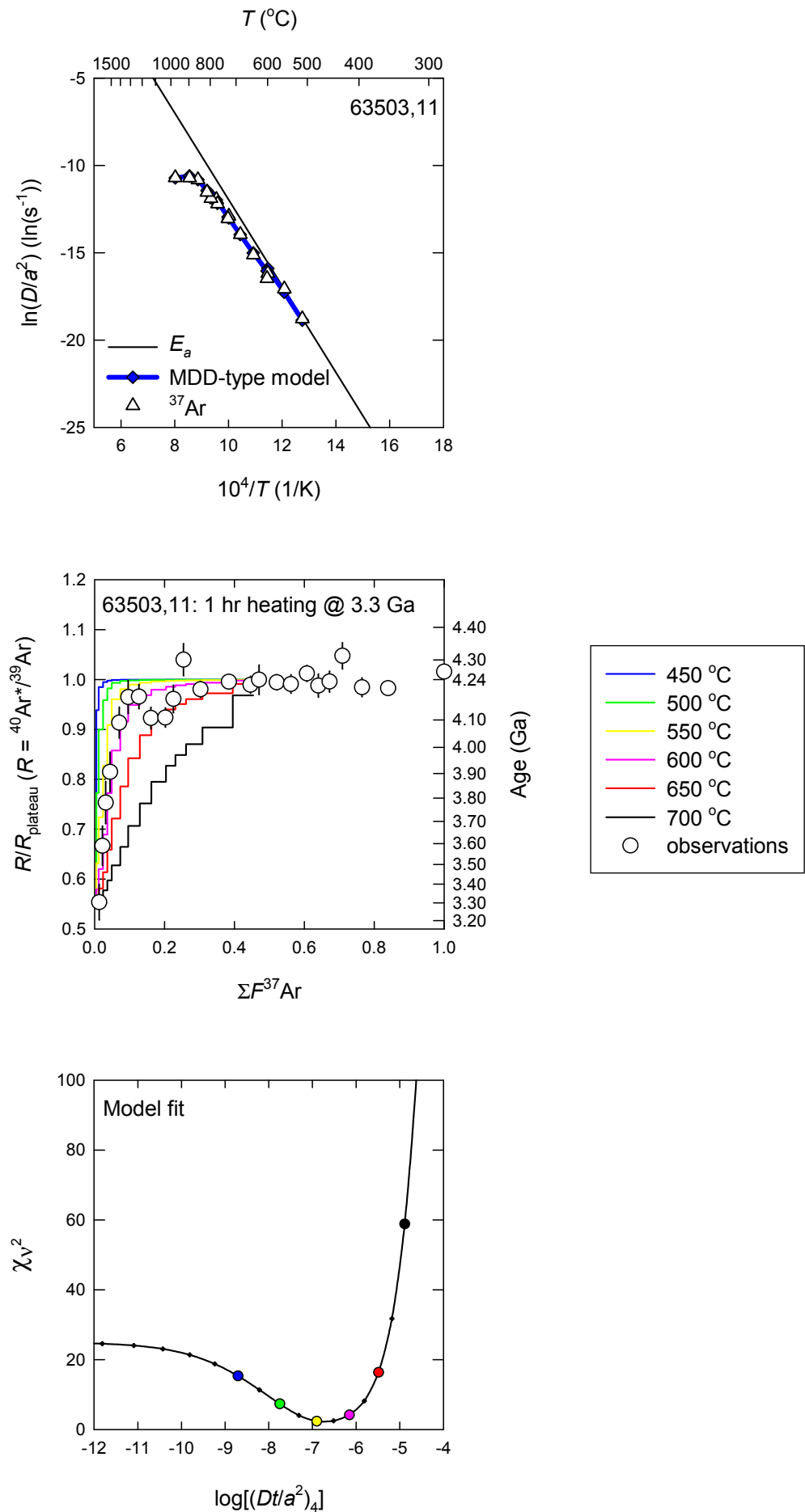


Figure S2f
Shuster et al., 2009

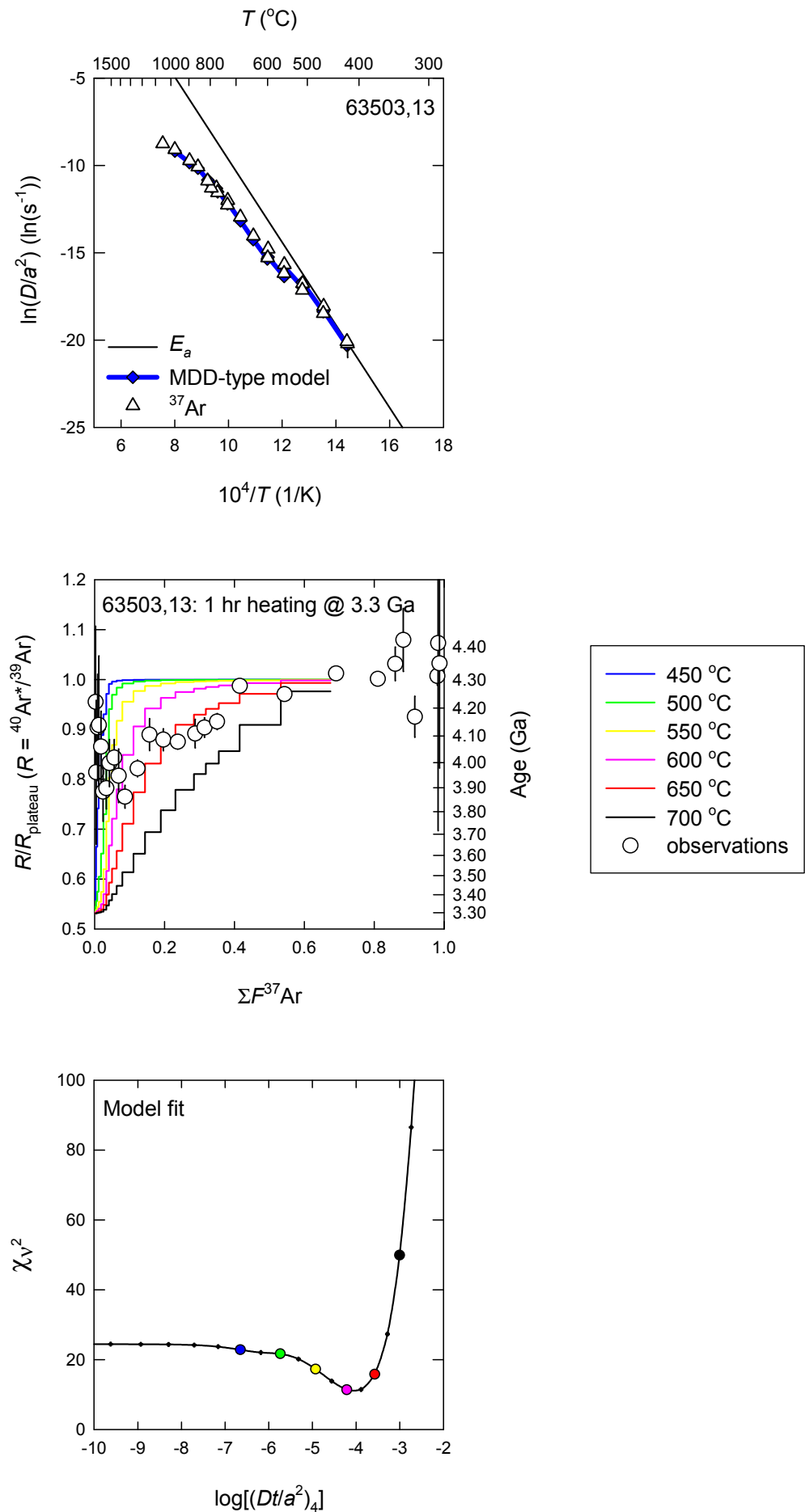


Figure S2g
Shuster et al., 2009

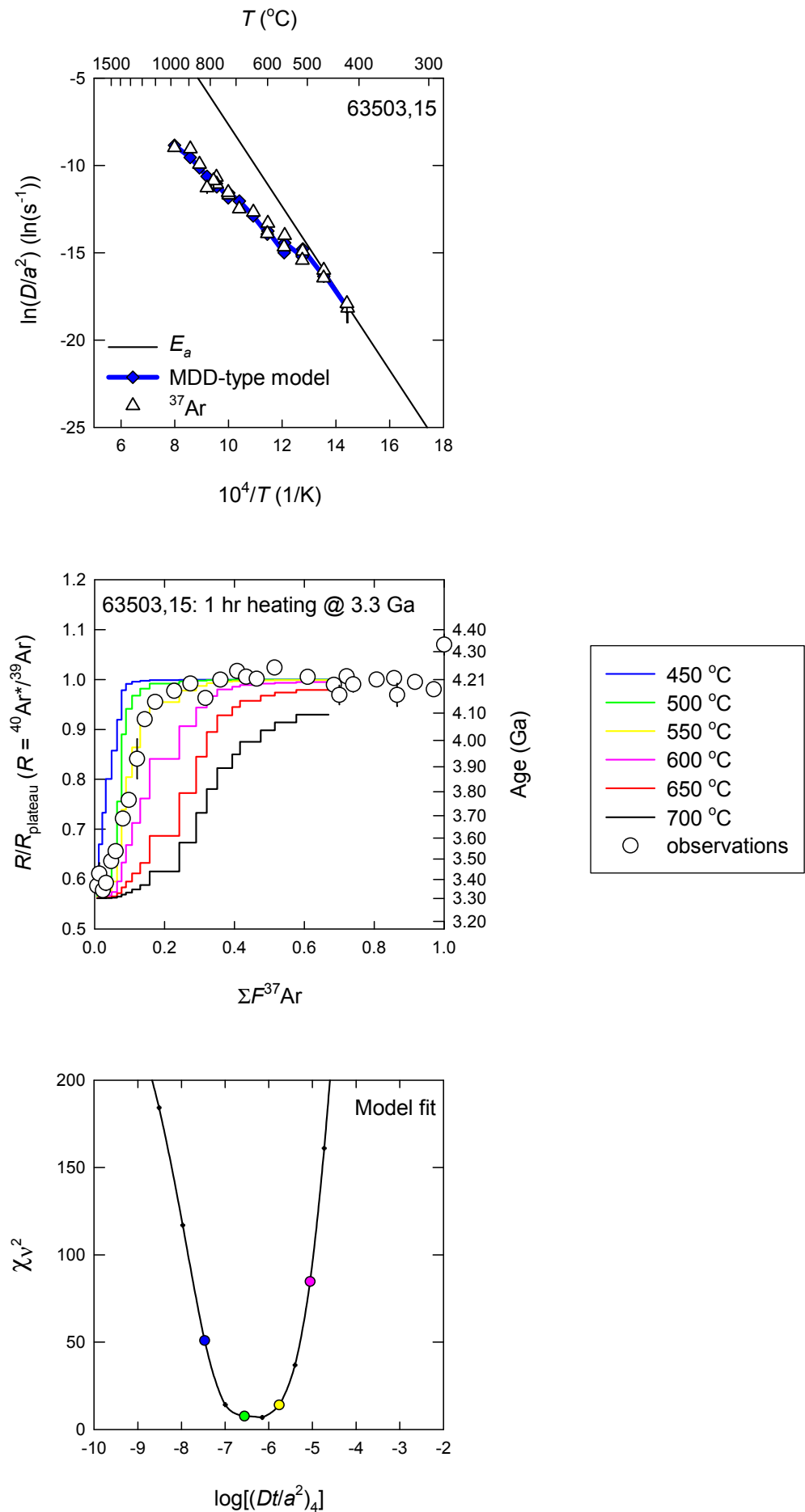
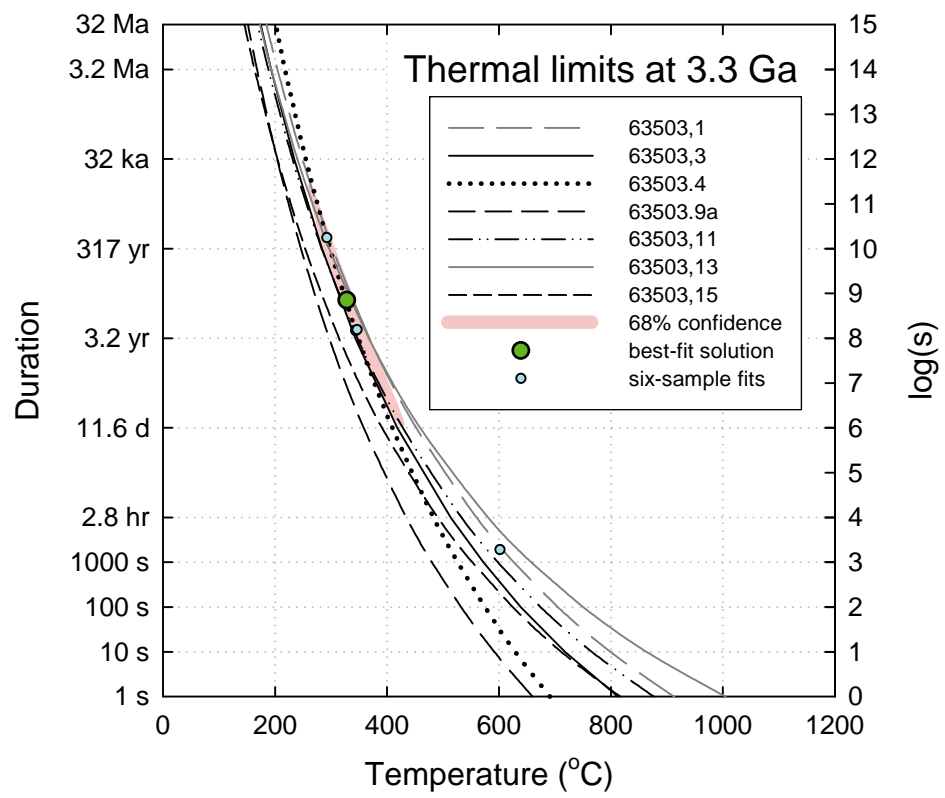


Figure S3
Shuster et al., 2009



COMPLETE ⁴⁰Ar/³⁹Ar INCREMENTAL HEATING RESULTS

Step #	Temp ^a (°C)	Time (sec)	⁴⁰ Ar / ³⁹ Ar ^b ± 1σ	³⁸ Ar / ³⁹ Ar ± 1σ	³⁷ Ar / ³⁹ Ar ± 1σ	³⁶ Ar / ³⁹ Ar ± 1σ	⁴⁰ Ar* / ³⁹ Ar ^c ± 1σ	³⁹ Ar _k (f)	³⁷ Ar _{Ca} (f)	⁴⁰ Ar* (%)	Ca/K	Apparent Age ^{d,e,f} ± 1σ Ma
63503,1												
1	n.d.	n.d.	n.d.	n.d.	33.81 ± 299.37	n.d.	n.d.	0.0100	0.0035		n.d.	n.d.
2	371	300	n.d.	n.d.	535.41 ± 1568.87	n.d.	n.d.	0.0001	0.0002		n.d.	n.d.
3	373	600	n.d.	n.d.	321.58 ± 300.52	n.d.	n.d.	0.0003	0.0004		n.d.	n.d.
4	417	300	169.02 ± 22.84	1.13 ± 0.16	194.43 ± 26.17	1.01 ± 0.14	195.43 ± 30.46	0.0027	0.0020	100	381	3282 ± 236
5	419	600	192.95 ± 18.45	1.34 ± 0.13	222.84 ± 21.27	1.17 ± 0.11	228.30 ± 25.77	0.0035	0.0030	100	437	3520 ± 175
6	462	300	180.11 ± 8.30	1.27 ± 0.06	208.03 ± 9.61	1.09 ± 0.05	210.55 ± 11.33	0.0088	0.0071	100	408	3396 ± 83
7	465	600	182.22 ± 8.84	1.26 ± 0.07	208.95 ± 10.14	1.08 ± 0.05	213.17 ± 12.08	0.0087	0.0071	100	410	3415 ± 88
8	505	300	170.27 ± 5.00	1.18 ± 0.04	197.92 ± 5.90	0.99 ± 0.03	197.42 ± 6.71	0.0133	0.0102	100	388	3298 ± 53
9	509	600	188.12 ± 6.62	1.31 ± 0.05	224.52 ± 8.08	1.10 ± 0.04	222.91 ± 9.29	0.0122	0.0107	100	440	3483 ± 65
10	552	300	180.03 ± 4.16	1.25 ± 0.03	224.98 ± 5.52	1.10 ± 0.03	213.40 ± 5.85	0.0194	0.0169	100	441	3416 ± 44
11	554	600	173.69 ± 3.98	1.26 ± 0.03	211.13 ± 5.00	1.07 ± 0.02	203.56 ± 5.46	0.0218	0.0179	100	414	3344 ± 43
12	595	300	189.42 ± 2.99	1.43 ± 0.02	234.48 ± 4.03	1.20 ± 0.02	226.30 ± 4.27	0.0281	0.0256	100	460	3507 ± 32
13	598	600	196.60 ± 3.22	1.43 ± 0.03	236.75 ± 4.08	1.25 ± 0.02	235.32 ± 4.62	0.0291	0.0267	100	464	3567 ± 33
14	640	300	198.40 ± 2.98	1.49 ± 0.02	243.33 ± 4.04	1.33 ± 0.02	238.78 ± 4.34	0.0374	0.0353	100	477	3590 ± 31
15	684	300	205.50 ± 2.36	1.56 ± 0.02	247.12 ± 2.96	1.46 ± 0.02	248.11 ± 3.45	0.0700	0.0672	100	484	3650 ± 25
16	724	150	220.28 ± 2.36	1.68 ± 0.02	269.82 ± 3.08	1.67 ± 0.02	271.12 ± 3.60	0.0555	0.0581	100	529	3789 ± 24
17	726	300	219.75 ± 2.29	1.69 ± 0.02	268.12 ± 3.29	1.61 ± 0.02	270.08 ± 3.50	0.0638	0.0665	100	526	3783 ± 24
18	766	150	226.43 ± 2.14	1.77 ± 0.02	279.00 ± 3.07	1.77 ± 0.02	280.89 ± 3.34	0.0624	0.0676	100	547	3846 ± 23
19	769	300	230.20 ± 2.40	1.77 ± 0.02	282.90 ± 3.39	1.66 ± 0.02	286.53 ± 3.76	0.0698	0.0767	100	554	3877 ± 24
20	787	150	224.62 ± 3.12	1.70 ± 0.03	277.10 ± 4.11	1.61 ± 0.02	278.20 ± 4.81	0.0387	0.0417	100	543	3830 ± 30
21	801	150	230.16 ± 3.50	1.76 ± 0.03	277.14 ± 4.28	1.60 ± 0.02	285.07 ± 5.38	0.0416	0.0448	100	543	3869 ± 33
22	841	150	236.35 ± 2.85	1.72 ± 0.02	279.39 ± 3.68	1.48 ± 0.02	293.31 ± 4.43	0.0579	0.0628	100	548	3914 ± 27
23	889	300	235.12 ± 2.13	1.59 ± 0.02	258.14 ± 2.87	1.19 ± 0.01	286.53 ± 3.21	0.0810	0.0812	100	506	3877 ± 22
24	975	300	237.76 ± 2.90	1.49 ± 0.02	244.85 ± 3.25	1.10 ± 0.01	286.51 ± 4.24	0.0571	0.0543	100	480	3877 ± 27
25	~1000	300	231.59 ± 3.44	1.41 ± 0.02	226.96 ± 3.43	1.24 ± 0.02	274.96 ± 4.85	0.0421	0.0371	100	445	3812 ± 31
26	~1100	300	234.56 ± 2.50	1.99 ± 0.02	285.64 ± 3.88	2.42 ± 0.03	292.66 ± 3.97	0.0649	0.0720	100	560	3911 ± 25
27	~1100	600	250.38 ± 5.67	2.72 ± 0.06	394.33 ± 9.11	3.08 ± 0.07	344.91 ± 10.82	0.0256	0.0392	100	773	4176 ± 53
28	~1200	300	353.04 ± 4.24	2.71 ± 0.03	264.30 ± 3.43	6.17 ± 0.07	432.49 ± 6.40	0.0587	0.0603	100	518	4548 ± 28
29	~1200	600	461.35 ± 204.44	2.31 ± 1.03	290.89 ± 128.96	4.43 ± 1.97	578.25 ± 321.06	0.0009	0.0010	100	570	5035 ± 940
30	>1300	600	219.26 ± 53.55	1.02 ± 0.26	140.49 ± 34.36	1.14 ± 0.28	242.99 ± 65.70	0.0016	0.0009	100	275	3617 ± 422
31	>1300	700	97.81 ± 4.22	0.40 ± 0.02	42.93 ± 1.96	0.46 ± 0.02	100.82 ± 4.48	0.0128	0.0021	100	84	2344 ± 59

Step #	Temp ^a (°C)	Time (sec)	⁴⁰ Ar / ³⁹ Ar ^b ± 1σ	³⁸ Ar / ³⁹ Ar ± 1σ	³⁷ Ar / ³⁹ Ar ± 1σ	³⁶ Ar / ³⁹ Ar ± 1σ	⁴⁰ Ar* / ³⁹ Ar ^c ± 1σ	³⁹ Ar _k (f)	³⁷ Ar _{Ca} (f)	⁴⁰ Ar* (%)	Ca/K	Apparent Age ^{d,e,g} ± 1σ Ma
63503,3												
1	402	300	214.15 ± 45.71	0.97 ± 0.22	170.64 ± 36.33	1.72 ± 0.37	242.96 ± 58.77	0.0010	0.0011	100	334	3618 ± 379
2	405	600	196.55 ± 26.48	0.86 ± 0.13	147.49 ± 19.84	1.45 ± 0.20	219.00 ± 32.84	0.0016	0.0016	100	289	3457 ± 233
3	456	300	189.06 ± 8.44	0.84 ± 0.04	138.17 ± 6.24	1.26 ± 0.06	209.14 ± 10.32	0.0057	0.0053	100	271	3387 ± 83
4	461	600	206.70 ± 11.48	0.88 ± 0.05	137.78 ± 7.69	1.21 ± 0.07	228.59 ± 14.02	0.0051	0.0047	100	270	3524 ± 101
5	503	300	209.60 ± 6.07	0.90 ± 0.03	142.22 ± 4.24	1.19 ± 0.03	232.59 ± 7.47	0.0096	0.0091	100	279	3550 ± 61
6	497	600	225.25 ± 7.86	0.87 ± 0.03	147.45 ± 5.20	1.18 ± 0.04	250.96 ± 9.74	0.0075	0.0074	100	289	3669 ± 70
7	545	300	223.41 ± 5.44	0.95 ± 0.02	158.69 ± 3.99	1.25 ± 0.03	251.10 ± 6.87	0.0125	0.0133	100	311	3670 ± 55
8	551	600	219.81 ± 5.36	0.90 ± 0.02	152.76 ± 3.84	1.21 ± 0.03	245.92 ± 6.71	0.0116	0.0118	100	299	3637 ± 55
9	600	300	210.76 ± 3.20	0.92 ± 0.02	150.22 ± 2.51	1.29 ± 0.02	235.33 ± 3.99	0.0191	0.0192	100	294	3569 ± 44
10	595	600	232.89 ± 4.88	1.02 ± 0.02	163.11 ± 3.55	1.43 ± 0.03	262.67 ± 6.21	0.0148	0.0162	100	320	3741 ± 51
11	639	300	234.40 ± 4.00	1.09 ± 0.02	165.61 ± 2.94	1.70 ± 0.03	264.89 ± 5.11	0.0220	0.0243	100	325	3754 ± 47
12	627	600	246.51 ± 4.62	1.13 ± 0.02	171.89 ± 3.37	1.78 ± 0.03	279.95 ± 5.96	0.0187	0.0215	100	337	3842 ± 49
13	684	300	238.83 ± 3.78	1.16 ± 0.02	166.69 ± 2.89	2.08 ± 0.03	270.12 ± 4.84	0.0294	0.0327	100	327	3785 ± 45
14	702	300	240.42 ± 2.42	1.21 ± 0.01	170.76 ± 1.99	2.30 ± 0.02	272.80 ± 3.13	0.0513	0.0587	100	335	3801 ± 40
15	776	150	250.17 ± 1.97	1.39 ± 0.01	181.00 ± 1.50	3.00 ± 0.02	286.17 ± 2.59	0.0553	0.0670	100	355	3877 ± 38
16	741	300	253.71 ± 2.65	1.29 ± 0.02	182.52 ± 2.08	2.28 ± 0.02	290.57 ± 3.48	0.0455	0.0556	100	358	3901 ± 41
17	809	150	253.92 ± 2.75	1.40 ± 0.02	185.87 ± 2.21	2.81 ± 0.03	291.58 ± 3.63	0.0529	0.0657	100	364	3906 ± 41
18	783	300	255.69 ± 2.62	1.24 ± 0.01	183.40 ± 2.02	1.97 ± 0.02	293.04 ± 3.44	0.0507	0.0622	100	359	3914 ± 40
19	795	150	259.58 ± 3.68	1.24 ± 0.02	184.18 ± 2.87	1.97 ± 0.03	297.68 ± 4.85	0.0273	0.0337	100	361	3940 ± 44
20	816	150	253.29 ± 3.07	1.19 ± 0.02	177.23 ± 2.44	1.88 ± 0.02	288.87 ± 4.00	0.0316	0.0374	100	347	3892 ± 42
21	857	150	255.40 ± 2.48	1.15 ± 0.01	178.39 ± 1.91	1.64 ± 0.02	291.54 ± 3.23	0.0562	0.0671	100	350	3906 ± 40
22	901	300	261.19 ± 1.84	1.01 ± 0.01	76.12 ± 2.77	0.95 ± 0.01	275.78 ± 2.11	0.1096	0.0558	100	149	3818 ± 38
23	982	300	259.53 ± 2.07	1.02 ± 0.01	58.29 ± 4.67	0.89 ± 0.01	270.48 ± 2.41	0.0887	0.0346	100	114	3787 ± 38
24	~1000	300	220.70 ± 2.08	1.07 ± 0.01	175.68 ± 2.03	1.18 ± 0.01	251.39 ± 2.72	0.0507	0.0596	100	344	3672 ± 39
25	~1100	300	221.28 ± 1.75	1.33 ± 0.01	65.88 ± 4.02	1.44 ± 0.01	231.90 ± 2.03	0.0724	0.0319	100	129	3546 ± 37
26	~1200	300	269.89 ± 4.04	1.74 ± 0.03	272.32 ± 4.51	1.78 ± 0.03	332.90 ± 6.21	0.0214	0.0389	100	534	4120 ± 47
27	~1200	600	287.60 ± 3.35	1.04 ± 0.01	186.68 ± 2.34	0.77 ± 0.01	330.48 ± 4.44	0.0402	0.0502	100	366	4108 ± 42
28	>1300	600	288.24 ± 2.54	1.06 ± 0.01	196.82 ± 1.91	0.79 ± 0.01	333.92 ± 3.42	0.0674	0.0887	100	386	4125 ± 40
29	>1300	600	250.71 ± 4.26	1.02 ± 0.02	181.60 ± 3.37	0.76 ± 0.01	286.92 ± 5.59	0.0202	0.0245	100	356	3881 ± 47

Step #	Temp ^a (°C)	Time (sec)	⁴⁰ Ar / ³⁹ Ar ^b ± 1σ	³⁸ Ar / ³⁹ Ar ± 1σ	³⁷ Ar / ³⁹ Ar ± 1σ	³⁶ Ar / ³⁹ Ar ± 1σ	⁴⁰ Ar* / ³⁹ Ar ^c ± 1σ	³⁹ Ar _k (f)	³⁷ Ar _{Ca} (f)	⁴⁰ Ar* (%)	Ca/K	Apparent Age ^{d,e,g} ± 1σ Ma
63503,4												
1	466	300	202.04 ± 9.54	1.81 ± 0.09	213.12 ± 15.73	5.94 ± 0.28	237.16 ± 13.35	0.0048	0.0043	100	418	3581 ± 94
2	511	300	207.15 ± 5.31	1.79 ± 0.05	209.30 ± 7.87	5.91 ± 0.15	242.41 ± 7.36	0.0130	0.0114	100	410	3615 ± 59
3	510	600	219.31 ± 3.82	1.84 ± 0.04	201.46 ± 7.36	5.86 ± 0.10	255.02 ± 5.34	0.0123	0.0104	100	395	3694 ± 48
4	557	300	238.47 ± 4.07	2.13 ± 0.04	217.61 ± 6.33	7.16 ± 0.12	280.96 ± 5.78	0.0182	0.0167	100	427	3847 ± 48
5	555	600	242.39 ± 3.62	2.26 ± 0.04	206.64 ± 5.54	7.84 ± 0.12	283.04 ± 5.04	0.0172	0.0150	100	405	3859 ± 46
6	600	300	259.92 ± 2.81	2.81 ± 0.03	212.31 ± 4.93	10.44 ± 0.11	304.91 ± 4.02	0.0225	0.0202	100	416	3978 ± 42
7	599	600	268.10 ± 3.33	2.99 ± 0.04	220.16 ± 4.96	11.45 ± 0.14	316.54 ± 4.78	0.0217	0.0202	100	432	4038 ± 44
8	645	300	281.68 ± 2.66	3.73 ± 0.04	222.56 ± 4.02	15.16 ± 0.14	333.23 ± 3.86	0.0269	0.0252	100	436	4121 ± 41
9	688	300	288.08 ± 1.98	4.40 ± 0.03	232.71 ± 3.10	18.79 ± 0.12	343.66 ± 2.96	0.0506	0.0497	100	456	4171 ± 39
10	726	150	291.53 ± 1.80	5.26 ± 0.03	239.62 ± 2.88	23.09 ± 0.14	349.78 ± 2.77	0.0469	0.0474	100	470	4200 ± 39
11	731	300	278.33 ± 1.84	4.29 ± 0.03	231.00 ± 2.95	17.63 ± 0.11	331.56 ± 2.73	0.0511	0.0498	100	453	4113 ± 39
12	774	150	293.55 ± 1.95	5.13 ± 0.04	231.89 ± 2.80	21.80 ± 0.14	349.95 ± 2.91	0.0499	0.0487	100	455	4201 ± 39
13	769	300	287.84 ± 2.70	3.88 ± 0.04	234.45 ± 2.93	14.98 ± 0.14	343.87 ± 3.92	0.0577	0.0570	100	460	4172 ± 41
14	794	150	289.13 ± 2.32	3.80 ± 0.04	227.36 ± 3.84	14.40 ± 0.11	343.39 ± 3.45	0.0320	0.0306	100	446	4170 ± 40
15	814	150	291.85 ± 2.00	3.48 ± 0.02	231.67 ± 3.17	12.88 ± 0.08	347.86 ± 2.97	0.0374	0.0365	100	454	4191 ± 39
16	856	150	292.41 ± 1.44	2.68 ± 0.01	225.15 ± 2.18	8.73 ± 0.04	346.66 ± 2.16	0.0617	0.0586	100	441	4185 ± 38
17	897	300	290.41 ± 1.81	1.57 ± 0.01	223.14 ± 2.15	2.84 ± 0.02	343.71 ± 2.63	0.0963	0.0906	100	437	4172 ± 38
18	978	300	294.44 ± 1.38	1.52 ± 0.01	228.14 ± 2.16	2.65 ± 0.01	349.93 ± 2.09	0.0661	0.0636	100	447	4201 ± 38
19	~1000	300	287.02 ± 2.35	2.52 ± 0.02	240.26 ± 3.30	7.55 ± 0.06	344.55 ± 3.53	0.0326	0.0331	100	471	4176 ± 40
20	~1100	300	277.34 ± 2.72	2.97 ± 0.03	245.05 ± 4.25	9.67 ± 0.09	334.27 ± 4.11	0.0280	0.0289	100	480	4126 ± 41
21	~1200	600	273.29 ± 2.72	2.35 ± 0.03	269.07 ± 4.95	5.99 ± 0.06	336.15 ± 4.32	0.0258	0.0293	100	527	4135 ± 42
22	~1200	300	285.12 ± 2.71	2.08 ± 0.02	288.78 ± 3.77	3.45 ± 0.03	356.71 ± 4.39	0.0500	0.0609	100	566	4232 ± 42
23	>1300	600	283.97 ± 1.87	1.28 ± 0.01	243.34 ± 2.74	1.08 ± 0.01	341.77 ± 2.83	0.0502	0.0515	100	477	4162 ± 39
24	>1300	300	290.13 ± 1.27	1.33 ± 0.01	259.85 ± 2.38	0.97 ± 0.00	354.08 ± 2.11	0.0833	0.0913	100	509	4220 ± 38
25	>1300	600	287.88 ± 1.97	1.35 ± 0.01	266.43 ± 3.27	1.02 ± 0.01	353.30 ± 3.15	0.0437	0.0491	100	522	4216 ± 39

Step #	Temp ^a (°C)	Time (sec)	⁴⁰ Ar / ³⁹ Ar ^b ± 1σ	³⁸ Ar / ³⁹ Ar ± 1σ	³⁷ Ar / ³⁹ Ar ± 1σ	³⁶ Ar / ³⁹ Ar ± 1σ	⁴⁰ Ar* / ³⁹ Ar ^c ± 1σ	³⁹ Ar _k (f)	³⁷ Ar _{Ca} (f)	⁴⁰ Ar* (%)	Ca/K	Apparent Age ^{d,e,f} ± 1σ Ma
63503,9a												
1	374	300	n.d.	n.d.	311.90 ± 2656.82	n.d.	n.d.	0.00003	0.00004		n.d.	n.d.
2	374	600	n.d.	n.d.	n.d. ± n.d.	n.d.	n.d.	n.d.	0.00035		n.d.	n.d.
3	421	300	n.d.	n.d.	147.89 ± 36.24	n.d.	n.d.	0.00130	0.00081		n.d.	n.d.
4	421	600	n.d.	n.d.	131.42 ± 35.48	n.d.	n.d.	0.00126	0.00070		n.d.	n.d.
5	465	300	254.39 ± 21.72	0.97 ± 0.09	119.34 ± 12.79	1.75 ± 0.15	277.40 ± 25.85	0.00334	0.00168	100	234	3826 ± 148
6	466	600	313.30 ± 34.91	1.13 ± 0.14	142.16 ± 19.28	2.16 ± 0.25	347.65 ± 43.06	0.00246	0.00147	100	279	4189 ± 202
7	510	300	324.46 ± 27.61	1.24 ± 0.12	181.57 ± 17.20	2.42 ± 0.21	371.31 ± 36.20	0.00355	0.00272	100	356	4296 ± 160
8	511	600	332.65 ± 29.13	1.37 ± 0.13	190.71 ± 18.89	2.40 ± 0.21	383.48 ± 38.78	0.00334	0.00268	100	374	4349 ± 167
9	554	300	259.60 ± 12.37	1.24 ± 0.07	169.14 ± 9.37	2.12 ± 0.10	294.18 ± 15.90	0.00637	0.00454	100	332	3919 ± 87
10	555	600	293.95 ± 12.97	1.31 ± 0.07	196.70 ± 10.09	2.49 ± 0.11	340.49 ± 17.43	0.00566	0.00469	100	386	4155 ± 84
11	600	300	280.34 ± 10.46	1.39 ± 0.06	193.56 ± 8.19	2.96 ± 0.11	323.91 ± 13.98	0.00849	0.00692	100	379	4074 ± 71
12	599	600	312.32 ± 12.60	1.57 ± 0.07	222.98 ± 10.00	3.24 ± 0.13	369.60 ± 17.67	0.00783	0.00736	100	437	4289 ± 79
13	642	300	295.38 ± 9.11	1.56 ± 0.05	216.50 ± 7.28	3.65 ± 0.11	347.69 ± 12.63	0.01120	0.01021	100	424	4189 ± 61
14	685	300	293.97 ± 4.64	1.64 ± 0.03	214.33 ± 4.00	3.97 ± 0.06	345.42 ± 6.43	0.02430	0.02195	100	420	4178 ± 33
15	724	150	296.30 ± 5.12	1.74 ± 0.03	220.16 ± 4.30	4.37 ± 0.08	349.82 ± 7.15	0.02147	0.01992	100	432	4199 ± 36
16	731	300	292.01 ± 4.91	1.63 ± 0.03	217.53 ± 4.19	3.54 ± 0.06	344.02 ± 6.83	0.02451	0.02246	100	426	4172 ± 35
17	767	150	301.18 ± 5.85	1.73 ± 0.04	234.77 ± 4.96	3.95 ± 0.08	359.90 ± 8.37	0.02355	0.02330	100	460	4245 ± 40
18	771	300	297.44 ± 5.15	1.45 ± 0.03	225.98 ± 4.41	2.59 ± 0.05	352.86 ± 7.27	0.02784	0.02651	100	443	4213 ± 36
19	807	150	304.04 ± 6.15	1.40 ± 0.03	225.64 ± 5.15	1.96 ± 0.04	360.59 ± 8.68	0.01858	0.01766	100	442	4248 ± 41
20	845	150	310.06 ± 4.97	1.29 ± 0.02	231.52 ± 4.06	1.44 ± 0.02	369.52 ± 7.09	0.03142	0.03066	100	454	4288 ± 34
21	897	300	293.97 ± 2.66	1.16 ± 0.01	223.55 ± 3.03	0.94 ± 0.01	348.04 ± 3.80	0.06876	0.06477	100	438	4190 ± 22
22	973	300	302.38 ± 3.04	1.17 ± 0.01	232.42 ± 3.09	1.02 ± 0.01	360.64 ± 4.39	0.07054	0.06909	100	456	4248 ± 24
23	~1000	300	302.78 ± 4.36	1.19 ± 0.02	224.21 ± 3.48	1.23 ± 0.02	358.67 ± 6.13	0.04627	0.04371	100	439	4239 ± 31
24	~1100	300	281.08 ± 3.26	1.30 ± 0.02	240.54 ± 3.26	1.30 ± 0.02	337.51 ± 4.73	0.04635	0.04698	100	471	4141 ± 26
25	~1100	600	293.15 ± 9.44	1.18 ± 0.04	230.94 ± 8.18	0.99 ± 0.03	349.19 ± 13.41	0.01089	0.01060	100	453	4196 ± 64
26	~1200	300	298.38 ± 2.12	1.26 ± 0.01	246.04 ± 2.45	0.94 ± 0.01	359.92 ± 3.17	0.16999	0.17624	100	482	4245 ± 19
27	~1200	600	286.03 ± 2.39	1.31 ± 0.01	255.40 ± 2.72	0.96 ± 0.01	347.76 ± 3.60	0.09883	0.10636	100	501	4189 ± 21
28	~1300	300	286.96 ± 2.72	1.33 ± 0.01	260.49 ± 3.00	0.99 ± 0.01	350.40 ± 4.13	0.07250	0.07958	100	511	4201 ± 23
29	>1300	300	284.45 ± 3.03	1.33 ± 0.02	263.22 ± 3.10	0.99 ± 0.01	348.14 ± 4.59	0.06616	0.07338	100	516	4191 ± 25
30	>1300	600	284.70 ± 2.69	1.25 ± 0.01	236.91 ± 2.86	0.97 ± 0.01	340.82 ± 3.75	0.12323	0.12302	100	464	4156 ± 22

Step #	Temp ^a (°C)	Time (sec)	⁴⁰ Ar / ³⁹ Ar ^b ± 1σ	³⁸ Ar / ³⁹ Ar ± 1σ	³⁷ Ar / ³⁹ Ar ± 1σ	³⁶ Ar / ³⁹ Ar ± 1σ	⁴⁰ Ar* / ³⁹ Ar ^c ± 1σ	³⁹ Ar _k (f)	³⁷ Ar _{Ca} (f)	⁴⁰ Ar* (%)	Ca/K	Apparent Age ^{d,e,f} ± 1σ Ma
63503,11												
1	511	300	146.75 ± 12.15	1.10 ± 0.09	257.10 ± 21.15	0.98 ± 0.08	178.68 ± 17.91	0.00516	0.00493	100	504	3148 ± 150
2	555	300	160.41 ± 8.45	1.24 ± 0.07	275.03 ± 14.43	1.11 ± 0.06	198.32 ± 12.83	0.00744	0.00762	100	539	3305 ± 99
3	599	300	191.99 ± 9.19	1.48 ± 0.07	281.67 ± 13.61	1.34 ± 0.06	238.72 ± 14.16	0.00903	0.00947	100	552	3589 ± 93
4	601	600	215.75 ± 9.77	1.63 ± 0.08	287.99 ± 13.20	1.48 ± 0.07	269.73 ± 15.23	0.00863	0.00919	100	564	3781 ± 90
5	642	300	232.15 ± 9.08	1.77 ± 0.07	294.02 ± 11.57	1.60 ± 0.06	291.77 ± 14.32	0.01151	0.01255	100	576	3906 ± 79
6	685	300	255.80 ± 6.88	1.89 ± 0.05	313.78 ± 8.65	1.80 ± 0.05	327.14 ± 11.26	0.02261	0.02633	100	615	4090 ± 57
7	726	150	270.42 ± 7.26	1.86 ± 0.05	313.01 ± 8.65	1.91 ± 0.05	345.61 ± 11.88	0.02222	0.02586	100	613	4179 ± 57
8	729	300	271.41 ± 5.45	1.88 ± 0.04	309.92 ± 6.49	1.69 ± 0.03	345.93 ± 8.88	0.02658	0.03059	100	607	4181 ± 44
9	774	150	263.11 ± 4.92	1.76 ± 0.04	293.29 ± 5.75	1.64 ± 0.03	330.48 ± 7.80	0.03154	0.03434	100	575	4106 ± 40
10	770	300	264.57 ± 4.49	1.75 ± 0.03	288.44 ± 5.29	1.46 ± 0.02	330.91 ± 7.06	0.03829	0.04095	100	565	4109 ± 37
11	796	150	275.84 ± 6.36	1.78 ± 0.04	285.87 ± 6.95	1.45 ± 0.03	344.23 ± 9.93	0.02192	0.02324	100	560	4173 ± 49
12	814	150	294.39 ± 7.15	1.84 ± 0.05	301.52 ± 7.76	1.49 ± 0.04	372.43 ± 11.49	0.02579	0.02886	100	591	4301 ± 52
13	855	150	282.05 ± 3.80	1.68 ± 0.02	282.99 ± 4.56	1.31 ± 0.02	351.10 ± 5.96	0.04622	0.04855	100	555	4205 ± 31
14	897	300	290.81 ± 2.96	1.56 ± 0.02	265.52 ± 3.02	1.17 ± 0.01	356.62 ± 4.49	0.08232	0.08113	100	520	4230 ± 24
15	974	300	293.51 ± 4.22	1.49 ± 0.02	247.20 ± 3.89	1.06 ± 0.02	354.39 ± 6.18	0.06794	0.06230	100	485	4220 ± 31
16	~1000	300	293.75 ± 7.17	1.56 ± 0.04	258.30 ± 6.73	1.19 ± 0.03	358.02 ± 10.67	0.02569	0.02466	100	506	4237 ± 50
17	~1100	300	290.85 ± 3.63	1.60 ± 0.02	263.96 ± 3.57	1.23 ± 0.02	356.19 ± 5.48	0.05158	0.05050	100	517	4228 ± 28
18	~1100	600	292.88 ± 4.55	1.49 ± 0.03	251.59 ± 4.30	1.09 ± 0.02	354.94 ± 6.70	0.04325	0.04037	100	493	4222 ± 33
19	~1200	300	301.91 ± 4.07	1.40 ± 0.02	240.48 ± 3.58	1.03 ± 0.01	362.49 ± 5.90	0.05128	0.04579	100	471	4257 ± 30
20	~1200	600	293.22 ± 5.74	1.42 ± 0.03	246.48 ± 5.02	1.06 ± 0.02	353.83 ± 8.36	0.03620	0.03309	100	483	4217 ± 41
21	~1200	600	293.89 ± 5.12	1.55 ± 0.03	253.24 ± 4.69	1.10 ± 0.02	356.66 ± 7.55	0.03412	0.03205	100	496	4230 ± 37
22	~1200	300	301.85 ± 6.12	1.66 ± 0.04	281.34 ± 6.00	1.21 ± 0.02	375.21 ± 9.49	0.03531	0.03689	100	551	4313 ± 43
23	~1300	300	285.49 ± 4.48	1.62 ± 0.03	273.82 ± 4.45	1.16 ± 0.02	352.59 ± 6.87	0.05515	0.05606	100	537	4212 ± 34
24	~1300	600	289.96 ± 3.14	1.52 ± 0.02	253.19 ± 3.28	1.11 ± 0.01	351.88 ± 4.65	0.07905	0.07427	100	496	4208 ± 25
25	>1300	300	296.02 ± 2.02	1.60 ± 0.01	268.27 ± 2.17	1.17 ± 0.01	363.86 ± 3.11	0.16118	0.16042	100	526	4263 ± 19

Step #	Temp ^a (°C)	Time (sec)	⁴⁰ Ar / ³⁹ Ar ^b ± 1σ	³⁸ Ar / ³⁹ Ar ± 1σ	³⁷ Ar / ³⁹ Ar ± 1σ	³⁶ Ar / ³⁹ Ar ± 1σ	⁴⁰ Ar* / ³⁹ Ar ^c ± 1σ	³⁹ Ar _k (f)	³⁷ Ar _{Ca} (f)	⁴⁰ Ar* (%)	Ca/K	Apparent Age ^{d,e,f} ± 1σ Ma
63503,13												
1	420	300	257.56 ± 29.96	12.41 ± 1.42	394.16 ± 46.69	10.49 ± 1.19	354.73 ± 56.38	0.00279	0.00241	100	773	4221 ± 259
2	421	600	226.02 ± 30.37	11.42 ± 1.49	362.76 ± 48.99	9.92 ± 1.29	302.21 ± 53.60	0.00245	0.00195	100	711	3962 ± 285
3	466	300	232.46 ± 19.27	12.67 ± 1.03	442.62 ± 36.47	10.85 ± 0.88	335.74 ± 39.71	0.00407	0.00394	100	868	4132 ± 192
4	466	600	229.71 ± 24.08	13.91 ± 1.43	459.59 ± 48.06	11.58 ± 1.19	337.52 ± 51.43	0.00331	0.00333	100	901	4141 ± 248
5	511	300	218.95 ± 12.48	12.99 ± 0.72	458.33 ± 26.12	11.13 ± 0.62	321.29 ± 26.53	0.00614	0.00616	100	898	4061 ± 134
6	511	600	202.02 ± 11.09	13.04 ± 0.70	428.97 ± 23.63	10.69 ± 0.57	287.83 ± 22.20	0.00640	0.00602	100	841	3884 ± 124
7	555	300	198.73 ± 7.45	14.53 ± 0.52	454.04 ± 16.95	11.99 ± 0.43	290.35 ± 15.59	0.00955	0.00950	100	890	3898 ± 87
8	555	600	215.17 ± 8.66	14.56 ± 0.57	437.05 ± 17.81	12.30 ± 0.48	309.04 ± 17.62	0.00907	0.00869	100	857	3998 ± 93
9	598	300	210.87 ± 6.23	16.00 ± 0.46	469.79 ± 14.01	13.52 ± 0.39	313.10 ± 13.60	0.01317	0.01356	100	921	4019 ± 71
10	600	600	204.38 ± 9.39	16.63 ± 0.75	457.26 ± 21.13	13.96 ± 0.63	299.58 ± 20.05	0.01277	0.01279	100	896	3948 ± 108
11	642	300	197.09 ± 4.23	15.88 ± 0.33	440.20 ± 9.60	14.09 ± 0.29	283.96 ± 8.68	0.01859	0.01793	100	863	3863 ± 50
12	684	300	212.29 ± 2.93	16.72 ± 0.28	437.51 ± 9.47	15.02 ± 0.21	305.05 ± 6.49	0.03780	0.03623	100	858	3977 ± 36
13	730	150	222.77 ± 5.46	18.82 ± 0.46	468.50 ± 12.15	17.62 ± 0.43	330.33 ± 12.12	0.03310	0.03398	100	918	4106 ± 61
14	731	300	219.95 ± 3.85	18.55 ± 0.32	469.50 ± 8.29	16.33 ± 0.27	326.48 ± 8.46	0.03847	0.03958	100	920	4087 ± 44
15	774	150	221.26 ± 2.59	18.48 ± 0.22	459.06 ± 6.41	16.70 ± 0.19	324.93 ± 5.82	0.04114	0.04139	100	900	4079 ± 32
16	769	300	225.88 ± 4.99	18.47 ± 0.41	457.31 ± 10.42	15.08 ± 0.33	331.12 ± 10.83	0.04970	0.04980	100	896	4110 ± 54
17	795	150	230.68 ± 3.50	18.62 ± 0.29	449.88 ± 7.30	14.92 ± 0.22	335.62 ± 7.55	0.02728	0.02690	100	882	4131 ± 39
18	811	150	232.35 ± 2.88	18.11 ± 0.23	455.64 ± 6.21	14.12 ± 0.17	340.03 ± 6.31	0.03571	0.03565	100	893	4153 ± 33
19	855	150	246.35 ± 2.12	19.08 ± 0.16	471.94 ± 5.24	13.92 ± 0.11	366.59 ± 5.05	0.06298	0.06513	100	925	4275 ± 26
20	897	300	245.35 ± 2.25	18.28 ± 0.19	459.58 ± 4.88	12.38 ± 0.11	360.50 ± 5.22	0.12756	0.12846	100	901	4248 ± 27
21	976	300	251.05 ± 2.20	18.59 ± 0.16	477.75 ± 4.64	12.43 ± 0.11	375.85 ± 5.32	0.14094	0.14754	100	936	4316 ± 27
22	~1000	300	250.67 ± 2.06	18.43 ± 0.16	468.68 ± 4.04	12.49 ± 0.10	371.77 ± 4.88	0.11647	0.11961	100	919	4298 ± 25
23	~1100	300	257.09 ± 5.70	18.98 ± 0.42	473.14 ± 10.70	13.69 ± 0.30	383.04 ± 12.78	0.04801	0.04978	100	927	4347 ± 56
24	~1100	600	262.01 ± 10.07	19.84 ± 0.76	498.24 ± 19.17	13.70 ± 0.52	400.80 ± 23.56	0.02111	0.02304	100	977	4422 ± 98
25	~1200	300	220.73 ± 8.00	21.18 ± 0.46	514.50 ± 11.92	14.96 ± 0.33	343.59 ± 15.49	0.02911	0.03282	100	1008	4170 ± 74
26	~1200	600	247.20 ± 3.79	19.23 ± 0.18	487.77 ± 5.67	12.50 ± 0.11	373.98 ± 7.31	0.06053	0.06469	100	956	4308 ± 35
27	~1300	300	275.26 ± 84.55	17.27 ± 2.80	445.00 ± 73.55	11.87 ± 1.96	398.52 ± 139.83	0.00225	0.00220	100	872	4412 ± 578
28	~1300	300	268.43 ± 48.26	17.47 ± 1.62	431.42 ± 41.49	11.36 ± 1.08	383.39 ± 77.98	0.00382	0.00361	100	846	4349 ± 334
29	~1300	600	837.50 ± 22.98	0.75 ± 0.02	10.98 ± 1.53	3.39 ± 0.10	843.94 ± 23.32	0.02187	0.00053	100	22	5681 ± 50
30	~1300	300	611.82 ± 19.22	16.17 ± 0.43	421.69 ± 11.83	12.42 ± 0.33	865.46 ± 35.59	0.01385	0.01279	100	827	5725 ± 72

Step #	Temp ^a (°C)	Time (sec)	⁴⁰ Ar / ³⁹ Ar ^b ± 1σ	³⁸ Ar / ³⁹ Ar ± 1σ	³⁷ Ar / ³⁹ Ar ± 1σ	³⁶ Ar / ³⁹ Ar ± 1σ	⁴⁰ Ar* / ³⁹ Ar ^c ± 1σ	³⁹ Ar _k (f)	³⁷ Ar _{Ca} (f)	⁴⁰ Ar* (%)	Ca/K	Apparent Age ^{d,e,g} ± 1σ Ma
63503,15												
1	420	300	175.84 ± 4.46	1.65 ± 0.05	212.96 ± 5.97	4.60 ± 0.11	206.38 ± 6.10	0.0074	0.0067	100	417	3366 ± 57
2	421	600	181.25 ± 5.51	1.56 ± 0.06	225.86 ± 7.75	4.54 ± 0.14	214.99 ± 7.72	0.0063	0.0060	100	443	3429 ± 65
3	465	300	171.97 ± 3.03	1.71 ± 0.04	221.78 ± 4.43	4.88 ± 0.08	203.31 ± 4.20	0.0116	0.0108	100	435	3344 ± 46
4	465	600	174.81 ± 3.85	1.75 ± 0.04	232.32 ± 5.96	4.89 ± 0.11	208.46 ± 5.45	0.0091	0.0089	100	455	3382 ± 53
5	510	300	185.98 ± 2.62	1.89 ± 0.03	243.16 ± 3.87	5.52 ± 0.08	223.80 ± 3.80	0.0143	0.0146	100	477	3491 ± 43
6	511	600	192.19 ± 2.94	1.92 ± 0.03	240.46 ± 4.27	5.63 ± 0.08	230.75 ± 4.23	0.0128	0.0130	100	471	3538 ± 45
7	554	300	209.81 ± 2.55	2.22 ± 0.03	249.41 ± 3.50	7.02 ± 0.08	253.80 ± 3.75	0.0194	0.0204	100	489	3687 ± 42
8	555	600	221.29 ± 3.37	2.48 ± 0.04	245.95 ± 4.18	7.97 ± 0.12	266.91 ± 4.91	0.0161	0.0167	100	482	3766 ± 46
9	599	300	242.25 ± 9.46	3.10 ± 0.12	261.08 ± 10.26	11.04 ± 0.43	295.96 ± 14.12	0.0218	0.0240	100	512	3930 ± 84
10	600	600	263.78 ± 3.18	3.56 ± 0.04	267.41 ± 3.57	12.92 ± 0.15	323.99 ± 4.81	0.0193	0.0218	100	524	4076 ± 43
11	642	300	272.27 ± 2.68	4.19 ± 0.04	273.67 ± 3.11	16.65 ± 0.16	336.21 ± 4.15	0.0260	0.0300	100	536	4136 ± 41
12	688	600	279.54 ± 1.99	5.11 ± 0.04	269.38 ± 2.47	21.41 ± 0.15	343.93 ± 3.14	0.0482	0.0547	100	528	4173 ± 39
13	726	300	286.36 ± 2.11	6.13 ± 0.05	258.72 ± 2.81	27.12 ± 0.19	349.14 ± 3.26	0.0424	0.0462	100	507	4197 ± 39
14	728	300	280.70 ± 2.48	5.24 ± 0.05	247.39 ± 2.77	22.28 ± 0.19	338.98 ± 3.69	0.0413	0.0431	100	485	4149 ± 40
15	774	150	291.66 ± 2.29	6.28 ± 0.05	246.08 ± 2.56	27.13 ± 0.20	351.83 ± 3.42	0.0412	0.0427	100	482	4210 ± 40
16	773	300	294.68 ± 2.70	4.77 ± 0.04	254.37 ± 2.81	19.11 ± 0.17	357.96 ± 4.07	0.0446	0.0478	100	499	4238 ± 41
17	786	150	294.29 ± 2.97	4.37 ± 0.05	242.36 ± 2.78	17.26 ± 0.17	353.90 ± 4.33	0.0252	0.0257	100	475	4219 ± 42
18	814	300	294.62 ± 2.86	3.89 ± 0.04	236.22 ± 2.66	14.71 ± 0.14	352.49 ± 4.15	0.0308	0.0306	100	463	4213 ± 41
19	848	150	301.90 ± 1.90	2.83 ± 0.02	233.56 ± 1.97	9.34 ± 0.06	360.40 ± 2.80	0.0520	0.0512	100	458	4249 ± 39
20	893	150	298.49 ± 1.48	1.56 ± 0.01	225.23 ± 1.62	2.73 ± 0.01	353.88 ± 2.18	0.0999	0.0948	100	441	4219 ± 38
21	978	150	295.53 ± 1.37	1.46 ± 0.01	217.79 ± 1.44	2.52 ± 0.01	348.23 ± 1.99	0.0817	0.0750	100	427	4193 ± 38
22	~1050	300	289.44 ± 4.89	3.16 ± 0.06	218.07 ± 4.28	11.37 ± 0.19	341.14 ± 6.83	0.0170	0.0156	100	427	4159 ± 49
23	~1150	300	291.37 ± 3.17	3.91 ± 0.05	255.38 ± 3.30	15.08 ± 0.16	354.24 ± 4.76	0.0194	0.0209	100	501	4221 ± 43
24	~1150	300	288.34 ± 3.66	1.92 ± 0.03	248.55 ± 4.00	4.26 ± 0.05	348.54 ± 5.42	0.0178	0.0186	100	487	4194 ± 44
25	~1200	300	296.69 ± 1.36	1.48 ± 0.01	225.90 ± 1.31	2.44 ± 0.01	351.94 ± 2.01	0.0704	0.0670	100	443	4210 ± 38
26	~1200	600	298.19 ± 1.96	1.20 ± 0.01	223.39 ± 1.88	1.01 ± 0.01	352.99 ± 2.82	0.0534	0.0503	100	438	4215 ± 39
27	~1200	300	289.56 ± 5.82	1.17 ± 0.03	217.65 ± 5.27	1.02 ± 0.03	341.17 ± 8.12	0.0095	0.0087	100	427	4159 ± 53
28	~1250	600	293.76 ± 1.71	1.21 ± 0.01	232.01 ± 1.51	0.92 ± 0.01	350.24 ± 2.51	0.0523	0.0511	100	455	4202 ± 38
29	~1300	600	290.17 ± 1.67	1.21 ± 0.01	228.86 ± 1.88	0.90 ± 0.01	345.06 ± 2.45	0.0556	0.0536	100	449	4178 ± 38
30	>1300	300	321.42 ± 5.36	1.22 ± 0.02	210.97 ± 3.85	1.12 ± 0.02	376.65 ± 7.38	0.0332	0.0295	100	413	4321 ± 49

See next page for Table S1 footnotes.

Table S1 Footnotes:

- a Due to potential changes in Pt-Ir emissivity above 1000°C, the temperature calibration is valid only between 350 and 1000°C. Temperatures outside the range are approximate.
- b Isotopes corrected for blank and discrimination parameters
- c Isotopes corrected for blank, discrimination and interference parameters
- d All ages were calculated using the decay constants of Steiger and Jäger ($\lambda_{40K} = 5.543 \times 10^{-10} \text{ yr}^{-1}$) and corrected for ^{37}Ar and ^{39}Ar decay, using half lives of 35.2 days and 269 years, respectively. Age uncertainty includes analytical error in J-value determined using flux monitor Hb3gr and age = 1073.6 ± 8.8 Ma (Jourdan and Renne, 2007).
- e All ages calculated assuming initial $^{40}\text{Ar}/^{36}\text{Ar} = 0$, as inferred from "isochron" diagrams.
- f Irradiation parameter $J = 0.02645 \pm 0.00021$
- g Irradiation parameter $J = 0.02647 \pm 0.00059$

Apparent ages shown in bold indicate steps used to calculate the "plateau ages" reported in Table 1.

The ^{37}Ar release fractions and temperatures shown in bold indicate steps used in linear regressions to quantify Ar diffusion kinetics, although all steps were used to calculate values $\sigma D/a^2$.

n.d. means not determined or below detection limit

References

Steiger, R. H. & Jäger, E. Subcommission on Geochronology - Convention on Use of Decay Constants in Geochronology and Cosmochronology. *Earth and Planetary Science Letters* 36, 359-362 (1977).
Jourdan, F. & Renne, P. R. Age calibration of the Fish Canyon sanidine $^{40}\text{Ar}/^{39}\text{Ar}$ dating standard using primary K-Ar standards. *Geochimica Et Cosmochimica Acta* 71, 387-402 (2007).

Interfering isotope production ratios

$(^{40}\text{Ar}/^{39}\text{Ar})_{\text{K}}$	(7.30 ± 0.92)E-04
$(^{38}\text{Ar}/^{39}\text{Ar})_{\text{K}}$	(1.22 ± 0.00)E-02
$(^{37}\text{Ar}/^{39}\text{Ar})_{\text{K}}$	(2.24 ± 0.16)E-04
$(^{39}\text{Ar}/^{37}\text{Ar})_{\text{Ca}}$	(6.95 ± 0.09)E-04
$(^{38}\text{Ar}/^{37}\text{Ar})_{\text{Ca}}$	(1.96 ± 0.08)E-05
$(^{36}\text{Ar}/^{37}\text{Ar})_{\text{Ca}}$	(2.65 ± 0.02)E-04
$(^{36}\text{Cl}/^{38}\text{Cl})_{\text{Cl}}$	263 ± 2

Decay constants

$^{40}\text{K } \lambda_{\epsilon}$	(5.81 ± 0.00)E-11 a ⁻¹
$^{40}\text{K } \lambda_{\beta}$	(4.962 ± 0.000)E-10 a ⁻¹
^{39}Ar	(2.58 ± 0.03)E-03 a ⁻¹
^{37}Ar	(5.4300 ± 0.0063)E-02 a ⁻¹
$^{36}\text{Cl } \lambda_{\beta}$	(2.35 ± 0.02)E-06 a ⁻¹

Supplementary Table S2: Summary of representative published Apollo 16 and 17 40Ar/39Ar datasets

Apollo Mission	Reference	Sample name	"Edge Age" ^{a,b} (Ma)	(+/-)	Plateau Age ^{a,c} (Ma)	(+/-)
16	Norman et al. 2006	60315	1939	40	3868	31
16	Norman et al. 2006	60666	1399	100	-	-
16	Norman et al. 2006	61015	2411	9	3899	36
16	Norman et al. 2006	61156	2453	47	3749	36
16	Norman et al. 2006	61225	3297	55	3885	36
16	Norman et al. 2006	61225-2	3717	240	3907	15
16	Norman et al. 2006	61569	1705	37	3793	13
16	Norman et al. 2006	62235	2128	7	3876	32
16	Norman et al. 2006	62295	1998	246	3866	12
16	Norman et al. 2006	63506-2	3183	86	-	-
16	Norman et al. 2006	63525	-	-	3895	36
16	Norman et al. 2006	63525-2	3789	71	4190	24
16	Norman et al. 2006	63537	2175	173	3838	12
16	Norman et al. 2006	63545	1186	36	3839	23
16	Norman et al. 2006	63549-2	2035	148	3840	11
16	Norman et al. 2006	63596	2806	25	3860	13
16	Norman et al. 2006	64568	1946	119	3867	9
16	Norman et al. 2006	64576	2328	81	3852	10
16	Norman et al. 2006	64585	-	-	3962	15
16	Norman et al. 2006	64815	-	-	3886	9
16	Norman et al. 2006	64816	2071	35	3852	12
16	Norman et al. 2006	64817	3202	172	3835	18
16	Norman et al. 2006	65015	1837	25	3854	14
16	Norman et al. 2006	65785	2031	4	3826	20
16	Norman et al. 2006	66095	275	80	3676	16
16	Norman et al. 2006	68519	1084	13	-	-
16	Norman et al. 2006	69945	2207	37	3877	11
17	Dalrymple and Ryder, 1996	72395,96A	3634	4	3893	16
17	Dalrymple and Ryder, 1996	72558,7A	2224	4	-	-
17	Dalrymple and Ryder, 1996	73155,33E	3392	5	3854	16
17	Dalrymple and Ryder, 1996	73155,34A	-	-	3937	16
17	Dalrymple and Ryder, 1996	76315,150A	-	-	3900	16
17	Dalrymple and Ryder, 1996	77135,178A	2291	4	-	-
17	Dalrymple and Ryder, 1996	72353,7A	3521	13	3887	16
17	Dalrymple and Ryder, 1996	72255,238B	3065	4	3869	16
17	Dalrymple and Ryder, 1996	72255,248B	3030	4	3838	16
17	Dalrymple and Ryder, 1996	72255,255B	2141	23	3867	16
17	Dalrymple and Ryder, 1996	72255,256B	2269	4	-	-
17	Dalrymple and Ryder, 1996	72255,282B	3439	5	3951	17
17	Dalrymple and Ryder, 1996	72255,287B	2996	4	3835	16
17	Dalrymple and Ryder, 1996	72255,235B	3412	6	3850	16
17	Dalrymple and Ryder, 1996	72255,275B	3584	13	3861	16
17	Dalrymple and Ryder, 1996	72735,13A	1489	3	-	-
17	Dalrymple and Ryder, 1996	73155,33A	2169	4	3865	16
17	Dalrymple and Ryder, 1996	73155,33B	3136	4	3900	16
17	Dalrymple and Ryder, 1996	78527,6A	2791	5	4146	17
16	Maurer et al., 1978	63503,LA1	3571	110	3878	50
16	Maurer et al., 1978	63503,LB1	2724	350	-	-
16	Maurer et al., 1978	63503,LC1	3551	60	3868	40
16	Maurer et al., 1978	63503,LD1	3734	45	4051	50
16	Maurer et al., 1978	63503,LE1	3474	35	3859	40
16	Maurer et al., 1978	63503,LF1	3080	90	4070	100
16	Maurer et al., 1978	63503,LG1	3686	600	-	-
16	Maurer et al., 1978	63503,LH1	3118	250	4022	70
16	Maurer et al., 1978	63503,LI1	3061	200	3897	40
16	Maurer et al., 1978	63503,LK1	2781	250	3811	50
16	Maurer et al., 1978	63503,LM1	-	-	2241	30
16	Maurer et al., 1978	63503,LN1	3061	500	3878	40
16	Maurer et al., 1978	67603,ME1	2700	35	3772	50
16	Maurer et al., 1978	67603,MM1	3590	500	4041	50
16	Maurer et al., 1978	67603,MO1	3205	100	4032	60
16	Maurer et al., 1978	67603,MP1	3542	120	-	-
16	Maurer et al., 1978	67603,MQ1	3349	600	3840	60
16	Maurer et al., 1978	67703,NA1	2820	200	-	-
16	Maurer et al., 1978	67703,NC1	3244	50	3494	50
16	Maurer et al., 1978	67703,ND1	2164	20	3849	40

16	Maurer et al., 1978	67703,NG1	3080	45	3830	40
16	Maurer et al., 1978	67703,NI1	2911	30	3849	40
17	Huneke et al., 1973	74220,13	-	-	3500	50
17	Huneke et al., 1973	75083,3,3	2324	160	3654	90
17	Huneke et al., 1973	76055,6	3558	80	3915	40
17	Huneke et al., 1973	75055 plag	3325	190	3732	40
17	Huneke et al., 1973	75055 K-rich	2099	90	-	-
17	Huneke et al., 1973	75055 whole	1883	130	-	-
16	Huneke et al., 1973	68415,10 plag	3364	100	4031	40
16	Huneke et al., 1973	68415,10 whole	1913	40	3799	40
16	Schaeffer and Husain., 1973	68503,13,5	-	-	3955	50
16	Schaeffer and Husain., 1973	68503,13,6	-	-	3897	60
16	Schaeffer and Husain., 1973	68503,13,7	-	-	3974	50
16	Schaeffer and Husain., 1973	68503,16,1	2961	22	3916	50
16	Schaeffer and Husain., 1973	68503,16,12	-	-	3887	60
16	Schaeffer and Husain., 1973	68503,16,31	3638	53	3781	70
16	Schaeffer and Husain., 1973	68503,16,33	3487	197	3868	60
16	Schaeffer and Husain., 1973	67483,13,6	2822	222	-	-
16	Schaeffer and Husain., 1973	67483,13,8	-	-	4166	50
16	Schaeffer and Husain., 1973	67483,14,2	3505	100	4147	50
16	Schaeffer and Husain., 1973	67483,14,6	-	-	3964	80
16	Schaeffer and Husain., 1973	67483,14,7	-	-	4012	100
16	Schaeffer and Husain., 1973	67483,14,18	-	-	3955	70
16	Schaeffer and Husain., 1973	66043,2,4	3477	23	4041	50
16	Schaeffer and Husain., 1973	66043,2,5	-	-	3926	50
16	Schaeffer and Husain., 1973	66043,2,17	1536	23	3714	50
16	Schaeffer and Husain., 1973	63503,13,2	-	-	3897	70
16	Schaeffer and Husain., 1973	63503,13,7	2425	18	3916	60
16	Schaeffer and Husain., 1973	63503,15,3	-	-	3868	60
16	Jessberger et al., 1974	65015	3388	75	3925	10
16	Bernatowicz et al., 1986	67415	3300	100	3960	50
16	Marvin et al., 1987	67415	3350	150	3960	40
16	Schaeffer and Husain, 1974	60015,22	2607	69	3434	50
16	Schaeffer and Husain, 1974	60015,69	-	-	3444	60
16	Schaeffer and Husain, 1974	60025,86	3263	56	4118	60
16	Schaeffer and Husain, 1974	60025,86,1	3365	50	4080	60
17	Schaeffer and Husain, 1974	78503,7,1	2790	71	3878	20
17	Schaeffer and Husain, 1974	78503,8,12	1644	31	4041	30
16	Shuster et al., 2009	63503	3350	80	3870	30
16	Shuster et al., 2009	63503	3390	160	3870	200
16	Shuster et al., 2009	63503	3700	100	4190	70
16	Shuster et al., 2009	63503	3920	180	4210	180
16	Shuster et al., 2009	63503	3310	190	4140	80
16	Shuster et al., 2009	63503	3390	100	4300	180
16	Shuster et al., 2009	63503	3350	90	4210	140

^a All ages were calculated using the decay constants of Steiger and Jäger (1977) ($\lambda_{40K} = 5.543 \times 10^{-10} \text{ yr}^{-1}$).

^b The edge ages were calculated from initial steps unless the ages exceeded the plateau age or were within error of the plateau age.

^c Plateau ages are as reported in original citations unless corrected for the decay constant. Note that some "edge ages" are determined from datasets which do not define plateaus.

References

- Bernatowicz, T. J., Lindstrom, M. M. & Podosek, F. A. ⁴⁰Ar-³⁹Ar ages of Apollo 16 North Ray Crater Rocks and dimict breccias. *Proc. Lunar Sci. Conf.* 17, 42-43 (1986).
- Dalrymple, G. B. & Ryder, G. ⁴⁰Ar/³⁹Ar age spectra of Apollo 17 highlands breccia samples by laser step heating and the age of the Serenitatis basin. *Journal of Geophysical Research* 101, 26069-26084 (1996).
- Huneke, J. C., Jessberger, E. K., Podosek, F. A. & Wasserburg, G. J. ⁴⁰Ar/³⁹Ar measurements in Apollo 16 and 17 samples and the chronology of metamorphic and volcanic activity in the Taurus-Littrow region. *Proc. Lunar Sci. Conf.* 4 2, 1725-1756 (1973).
- Jessberger, E. K., Huneke, J. C. & Wasserburg, G. J. Evidence For A - 4.5 Aeon Age Of Plagioclase Clasts In A Lunar Highland Breccia. *Nature* 248, 199-202 (1974).
- Marvin, U. B., Lindstrom, M. M., Bernatowicz, T. J. & Podosek, F. A. The Composition and History of Breccia-67015 from North-Ray Crater. *Journal of Geophysical Research-Solid Earth and Planets* 92, E471-E490 (1987).
- Maurer, P. et al. Pre-Imbrian craters and basins - Ages, compositions and excavation depths of Apollo 16 breccias. *Geochim. Cosmochim. Acta* 42, 1687-1720 (1978).
- Norman, M. D., Duncan, R. A. & Huard, J. J. Identifying impact events within the lunar cataclysm from ⁴⁰Ar-³⁹Ar ages and compositions of Apollo 16 impact melt rocks. *Geochim. Cosmochim. Acta* 70, 6032-6049 (2006).
- Schaeffer, O. A. & Husain, L. Early lunar history: Ages of 2 to 4 mm soil fragments from the lunar highlands. *Proc. Lunar Sci. Conf.* 4, 1847-1863 (1973).
- Schaeffer, O. A. & Husain, L. Chronology of lunar basin formation. *Proc. Lunar Sci. Conf.* 5, 1541-1555 (1974).
- Steiger, R. H. & Jager, E. Subcommittee on Geochronology - Convention on Use of Decay Constants in Geochronology and Cosmochronology. *Earth and Planetary Science Letters* 36, 359-362 (1977).